THE EUROPEAN
PHYSICAL JOURNAL
SPECIAL TOPICS

Review

Photoproduction of mesons off nuclei

Electromagnetic excitations of the neutron and meson-nucleus interactions

B. Krusche[a]

Department of Physics, University of Basel, 4056 Basel, Switzerland

Abstract. Recent results for the photoproduction of mesons off nuclei are reviewed. These experiments have been performed for two major lines of research related to the properties of the strong interaction. The investigation of nucleon resonances requires light nuclei as targets for the extraction of the isospin composition of the electromagnetic excitations. This is done with quasi-free meson photoproduction off the bound neutron and supplemented with the measurement of coherent photoproduction reactions, serving as spin and/or isospin filters. Furthermore, photoproduction from light and heavy nuclei is a very efficient tool for the study of the interactions of mesons with nuclear matter and the in-medium properties of hadrons. Experiments are currently rapidly developing due to the combination of high quality tagged (and polarized) photon beams with state-of-the-art 4π detectors and polarized targets.

1 Introduction and overview of the research topics

During the last two decades, photoproduction of mesons has become a prime tool for the study of the properties of the strong interaction in the regime where this fundamental force cannot be treated with the methods of perturbation theory. It has almost completely replaced meson induced reactions like pion elastic scattering, which had previously dominated this field. On the experimental side, this development was triggered by the large progress in accelerator and detector technology which nowadays allows the measurement of the cross sections of electromagnetically induced reactions routinely with comparable or even better precision than hadron induced reactions, although the latter typically have cross sections which are three orders of magnitude larger. The experiments are centered at high duty electron beams, in particular CEBAF at Jlab in Newport News, at the ELSA accelerator in Bonn, at the MAMI accelerator in Mainz, at SPring-8 in Osaka, at LNS at Tohoku University in Sendai, and, until recently, also at the GRAAL facility at the ESRF in Grenoble.

The largest part of this program involves meson photo- or electro-production experiments off the free proton aiming at a better understanding of the structure

---

[a] e-mail: `Bernd.Krusche@unibas.ch`
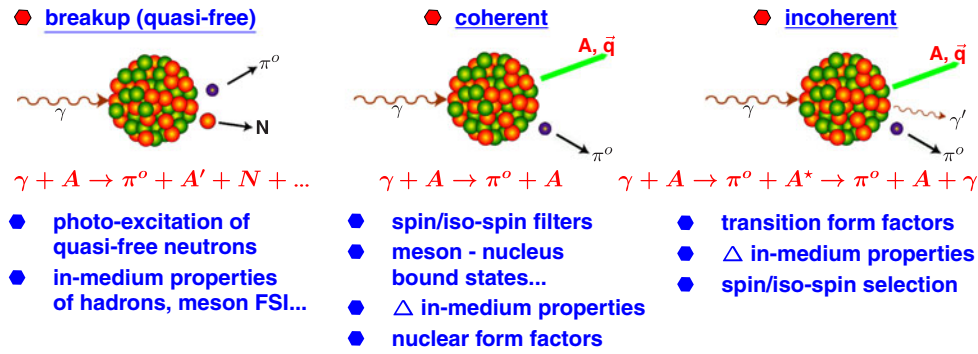
Fig. 1. Different nuclear meson production processes for the example of single π^0-photoproduction (see text).

and the excitation spectrum of the nucleon. However, there is also a very active and growing program studying nuclear targets. The physics topics of this program are diverse and the most important ones are summarized in Fig. 1.

Photoproduction of mesons off nuclei is mostly characterized by three types of final state. In the case of breakup reactions, at least one nucleon is removed from the nucleus. As we will discuss later, this type of process includes quasi-free meson production reactions, where the meson is produced on one 'participant' nucleon, while the rest of the nucleus acts as 'spectator'. This simple picture is mostly used for light nuclei, in particular the deuteron, where final state interaction effects (FSI) play a minor role. The study of meson photoproduction off the neutron can only be performed in this way. The methods for the extraction of elementary cross section of the neutron target and the recent results from such experiments are a central topic of this report. However, breakup reactions are also used in the case of heavier nuclei to study in-medium properties of hadrons and FSI effects, e.g. exploring the scaling behavior of the reaction cross sections in dependence on the nuclear mass number. A recent review of the in-medium properties of scalar and vector mesons derived from photoproduction and other reactions is given by Leupold, Mosel, and Metag [1]; results for the in-medium properties of nucleon resonances are summarized e.g. in [2].

Coherent meson photoproduction is characterized by a final state with the initial-state nucleus in its ground state. Exploring the spin and isospin quantum numbers of the nucleus can be used to project out specific parts of the elementary reaction amplitudes. However, with a few exceptions, typical cross sections are small and the experiments are so demanding that only few results are available up to now. Coherent meson production is also used as a doorway reaction for the search of meson-nucleus bound states. As an example we will discuss tentative evidence for η-mesic states. Coherent photoproduction of π^0 mesons was also used for the study of the in-medium properties of the $\Delta(1232)$ resonance (see e.g. [3,4]), and in a completely different context, for the extraction of nuclear mass form factors [5].

Incoherent production finally denotes the process where the final-state nucleus is excited (but otherwise identical with the initial state nucleus) and de-excites typically by emission of γ-radiation. Such processes provide additional selection possibilities as spin- and isospin filters (by selection of the final state quantum numbers), but are still almost unexplored due to the small reaction cross sections. Incoherent pion production can also contribute to the study of Δ-in-medium properties and give access to nuclear transition form factors. The first precise experimental study for incoherent photoproduction of π^0 mesons to the 4.4 MeV excited state of ^{12}C has been recently reported by Tarbert et al. from the Crystal Ball/TAPS collaboration at MAMI [6].

The main emphasis of this article will be on the study of the isospin degree of freedom of the nucleon excitation scheme via quasi-free meson photoproduction off the neutron and coherent photoproduction of light nuclei and on meson-nucleus interactions, in particular the search for meson-nucleus quasi-bound states.

1.1 Nucleon resonances

Understanding the properties of the strong interaction in the non-perturbative regime, where it gives rise to the observed hadron spectrum, is still a great challenge. One expects that, as in nuclear structure physics, the excitation spectrum of hadrons will reflect the main properties of the interaction, so that many efforts have been undertaken to study the excited states of the nucleon. However, so far, the results are not satisfactory. On the theory side, the only direct connection between baryon properties and Quantum Chromodynamics (QCD) has been established through the numerical method of lattice gauge theory. During the last few years, the progress in this field has been tremendous for the ground state properties of hadrons [7]. But first results for excited states [10], going beyond earlier quenched approximations [8,9], became available only very recently.

In a more indirect way, experimental observations and QCD are connected via QCD inspired quark models. However, in spite of their phenomenological successes, the basis of these models is still not well anchored. There is neither consent about the effective degrees of freedom nor about the residual quark - quark interactions (see e.g. Ref. [11,12] for detailed reviews). So far, a comparison of the experimentally known excitation spectrum of the nucleon to such model predictions does not clearly favor any of the different models. In fact, in most cases even the ordering of some of the lowest lying excitations is not reproduced. In particular, the $N(1440)P_{11}$ ('Roper') resonance and the first excited Δ, the $P_{33}(1600)$, are notoriously problematic. Furthermore, even the models with the fewest effective degrees of freedom predict many more states than have been observed, which is known as the 'missing resonance' problem. This problem is severe; only for very few combinations of quantum numbers has more than the lowest lying excited state been found experimentally so far. Nevertheless, it could also be rooted in trivial experimental bias. Most nucleon resonances have been established so far by elastic pion scattering, so that states that decouple from $N\pi$ are suppressed. Photon-induced reactions can avoid this bias when other final states than single pion production are also investigated. This is the main motivation for the world-wide experimental program for the study of photon-induced meson production reactions off the nucleon. As an example, Fig. 2 (left hand side) shows the contribution of different resonances to single π^0 and η-photoproduction at fairly low incident photon energies. While the extraction of the tiny contribution of the $S_{11}(1535)$ resonance to pion photoproduction requires complicated model analyses, this resonance completely dominates η-photoproduction in the threshold region [13,14], allowing significantly more detailed studies of this state. Following the same approach, photoproduction of heavier mesons like the η' has also been studied recently from the respective production threshold [15–17]. However, here the situation turned out to be less simple; first model analyses do not give conclusive results for the contributing resonances. In this, as in many other cases, differential cross section data alone do not sufficiently constrain the model analysis, which is the motivation for the large current efforts to measure single and double polarization observables.

Higher lying excited states may not only decay by single meson emission to the nucleon ground state but also via an intermediate excited states, giving rise to double or even triple meson production reactions. Making again the analogy to nuclear spectroscopy, it is evident that spectral information based only on the 'ground state'
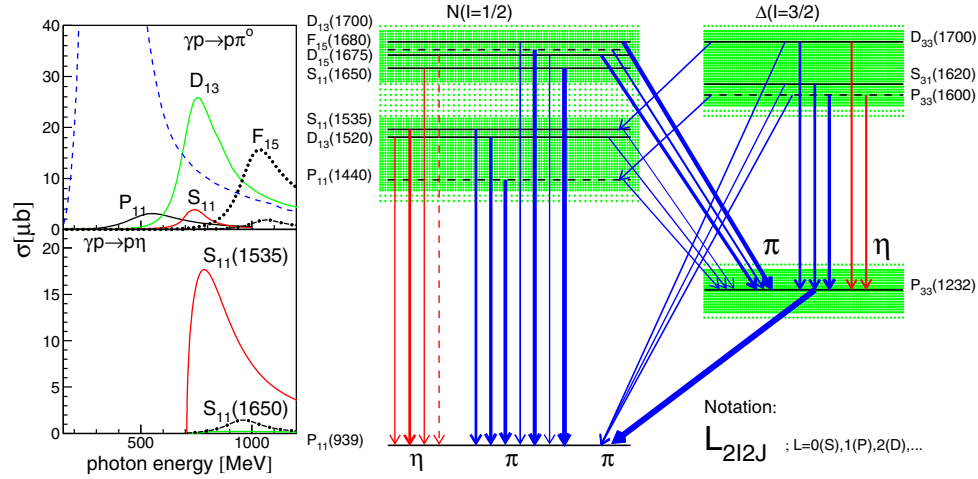
Fig. 2. Left hand side: contributions of different nucleon resonances to $\gamma p \rightarrow p\pi^0$ and $\gamma p \rightarrow p\eta$ (schematic). Right hand side: low energy excitation scheme of the nucleon. Isospin $I = 1/2$ $N^\star$ resonances left and isospin $I = 3/2$ Δ-resonances right. Typical decays are indicated.

decays of excited states is very incomplete. As indicated in the nucleon 'level-scheme' in Fig. 2 already states at moderate excitation energies can have substantial decay branching ratios to intermediate states and for higher excitation energies such decay modes will become more probable. Therefore multi-meson production reactions have also moved into the focus. Double pion production has recently been studied up to incident photon energies of 1.8 GeV [18–20]. Also in this case polarization observables are urgently needed to constrain the model analyses. First measurements of the beam-helicity asymmetry $I^\odot$ have revealed severe problems in the reaction models [21,22]. More recently, also the $\eta\pi$-channel has been studied, which has the additional advantage of isospin selectivity (η-mesons are only emitted in $N^\star \rightarrow N^{(\star)}$ and $\Delta^\star \rightarrow \Delta^{(\star)}$ transitions). First results point to a dominant contribution of one resonance at threshold [23–27], and possibly a parity doublet around $W \approx 1.9$ GeV [28].

In summary, an intensive experimental program is currently under way in particular at the CLAS facility at Jlab, the Crystal Barrel/TAPS experiment at ELSA, and the Crystal Ball/TAPS experiment at MAMI to measure differential cross sections, single and double polarization observables with polarized beams and polarized targets for many different single and double meson production reactions off the proton. The last missing degree of freedom in the experiments is the isospin dependence of the cross sections.

The electromagnetic interaction does not conserve isospin. The electromagnetic transition operator $\hat{A}$ can be split in an isoscalar part $\hat{S}$ and an isovector part $\hat{V}$, giving rise to three independent matrix elements [29] in the notation $\langle I_f, I_{f3}|\hat{A}|I_i, I_{i3}\rangle$:

$$A^{IS} = \langle \tfrac{1}{2}, \pm\tfrac{1}{12}|\hat{S}|\tfrac{1}{2}, \pm\tfrac{1}{2}\rangle, \quad \mp A^{IV} = \langle \tfrac{1}{2}, \pm\tfrac{1}{2}|\hat{V}|\tfrac{1}{2}, \pm\tfrac{1}{2}\rangle, \quad A^{V3} = \langle \tfrac{3}{2}, \pm\tfrac{1}{2}|\hat{V}|\tfrac{1}{2}, \pm\tfrac{1}{2}\rangle . \tag{1}$$

Photoproduction of isovector mesons like pions involves all three matrix elements, while only A^{IS} and A^{IV} contribute in the case of isoscalar mesons like the η. Nevertheless, in both cases at least one reaction on a neutron target must be measured
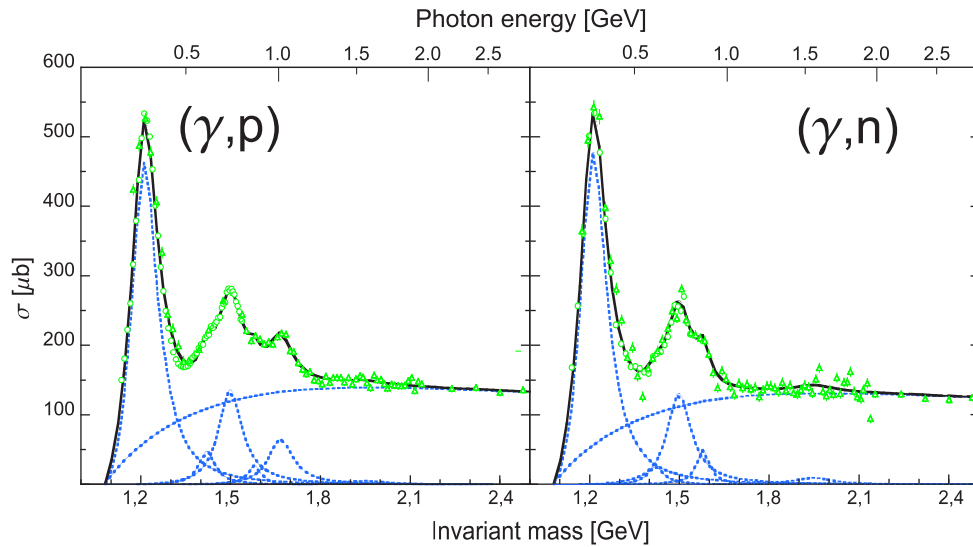
Fig. 3. Cross section for total photoabsorption on the proton (left hand side) and the neutron (right hand side) [32]. Points: measured data, curves: fit of Breit-Wigner shapes of nucleon resonances ($P_{33}(1232)$, $P_{11}(1440)$, $D_{13}(1520)$, $S_{11}(1535)$, $F_{15}(1680)$ (only for proton), and $F_{37}(1950)$) and a smoothly varying background.

for a unique isospin decomposition of the multipole amplitudes (see e.g. [30] for details). The situation for the excitation of nucleon resonances is different for $N^\star$- and Δ-states. The latter involve only the A^{V3} matrix element, so that they are excited identically on protons and neutrons, while the combination of A^{IS} and A^{IV} components leads in general to different electromagnetic couplings for protons and neutrons in the excitation of $N^\star$ states. In the limit of SU(3) symmetry in extreme cases $\gamma NN^\star$ transitions may even be completely forbidden for the proton but allowed for the neutron (Moorehouse selection rules [31]). Although due to the non-negligible spin-orbit mixing in the wave functions they are not strictly forbidden in more realistic models, they remain suppressed and can be better studied using neutron targets.

Already the measurement of total photoabsorption [32–34], reveals differences in the electromagnetic excitation of resonances on the proton and on the neutron (see Fig. 3). The bump-like structures of the second and third resonance region are quite different, but such inclusive measurements do not allow the extraction of detailed information about the isospin structure of the amplitudes.

The investigation of exclusive meson production reactions off the neutron is still much less advanced than for the proton case. The reason is that no free neutron targets exist so that only quasi-free photoproduction off the neutron bound in light nuclei and additionally coherent photoproduction from light nuclei can be used. The use of quasi-free reactions off bound nucleons involves two complications. Technically the experiments must detect the recoil nucleons. This is more or less straightforward for protons but more challenging for neutrons, so that in particular reactions with only neutral mesons in the final state are difficult to measure since detection probabilities for neutrons and achievable energy resolution are at best moderate. Furthermore, as is the case for all quasi-free measurements, the interpretation of the data must include nuclear effects like Fermi motion, re-scattering, and FSI, which leads to model dependent analyses and results.

As an example, the available entries from the SAID data base [35] for angular distributions of pion production off the nucleon are compared for the different isospin
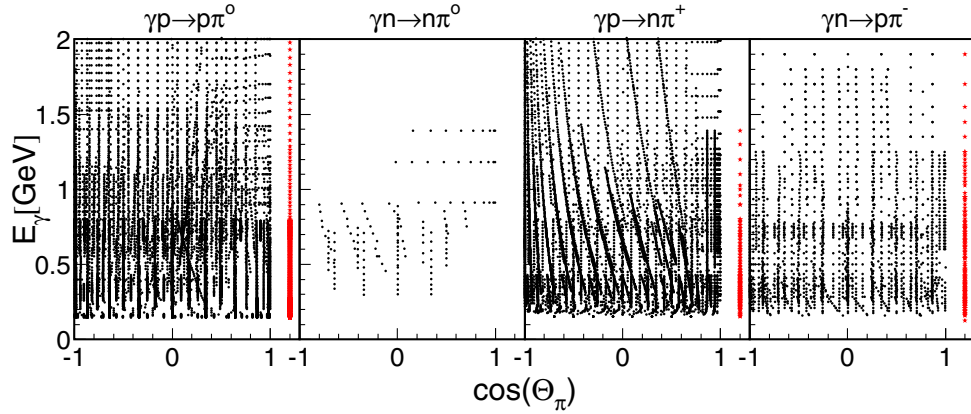
Fig. 4. Available data for angular distributions and total cross sections (red stars at $\cos(\theta_\pi) = 1.1$) for the photoproduction of pions off the nucleon.

channels in Fig. 4. The data base is quite extensive for the two reactions off the free proton. Results for the $\gamma n \to p\pi^-$ final state are less abundant but also available for a fairly complete angular range below incident photon energies of $1\,\mathrm{GeV}$, while the fully neutral final state $n\pi^0$ is basically unexplored. This is so because the reaction $\gamma d \to pp\pi^-$ with three charged particles in the final state can be easily studied. In fact most of these data go back to bubble chamber measurements from the early 1970's and have been analyzed with plane wave approximations assuming closure [36]. Only recently new data from the CLAS experiment have been published for this channel [37].

Since in principle the measurement of three of the four isospin channels allows the complete determination of the isospin structure of the amplitudes, one might ask at this point, whether the experimental efforts to measure also the fully neutral channel $n\pi^0$ are worthwhile. One answer is, that this trick works only for isovector mesons, while for the isoscalar ones like the η, η', ω,... photoproduction reactions with final state neutrons cannot be avoided. The other answer is, that even for isovector mesons like the pion the fully neutral final state carries important additional information for partial wave analysis. This is so, because not only resonance excitations contribute to the photoproduction reactions. Background terms like meson-pole terms, Kroll-Rudermann-like terms, diffractive t-channel contributions etc. must also be considered and can contribute differently to the isospin channels.

A very simple but instructive example is photoproduction of pions in the Δ-resonance region. Total cross sections are shown in Fig. 5. The only nucleon resonance that contributes significantly in this energy range is the $P_{33}(1232)$. It follows immediately from the isospin decomposition of the amplitude that as long as background terms are neglected (so that only A^{V3} contributes) the cross sections are related by

$$\sigma(\gamma p \to p\pi^0) = \sigma(\gamma n \to n\pi^0) = 2\sigma(\gamma p \to n\pi^+) = 2\sigma(\gamma n \to p\pi^-). \qquad (2)$$

But the measured cross sections show a completely different pattern due to the contribution of the background terms, which are much more important for the channels with charged pions since the photon does not couple directly to the neutral pion. The contribution of the Δ-resonance (dashed-curves) extracted by the MAID model [41] obeys of course the above relation since this is built into the model. Even in this most simple case, additional experimental information for the $n\pi^0$ final state would be helpful in order to test the model. In more complicated cases, involving
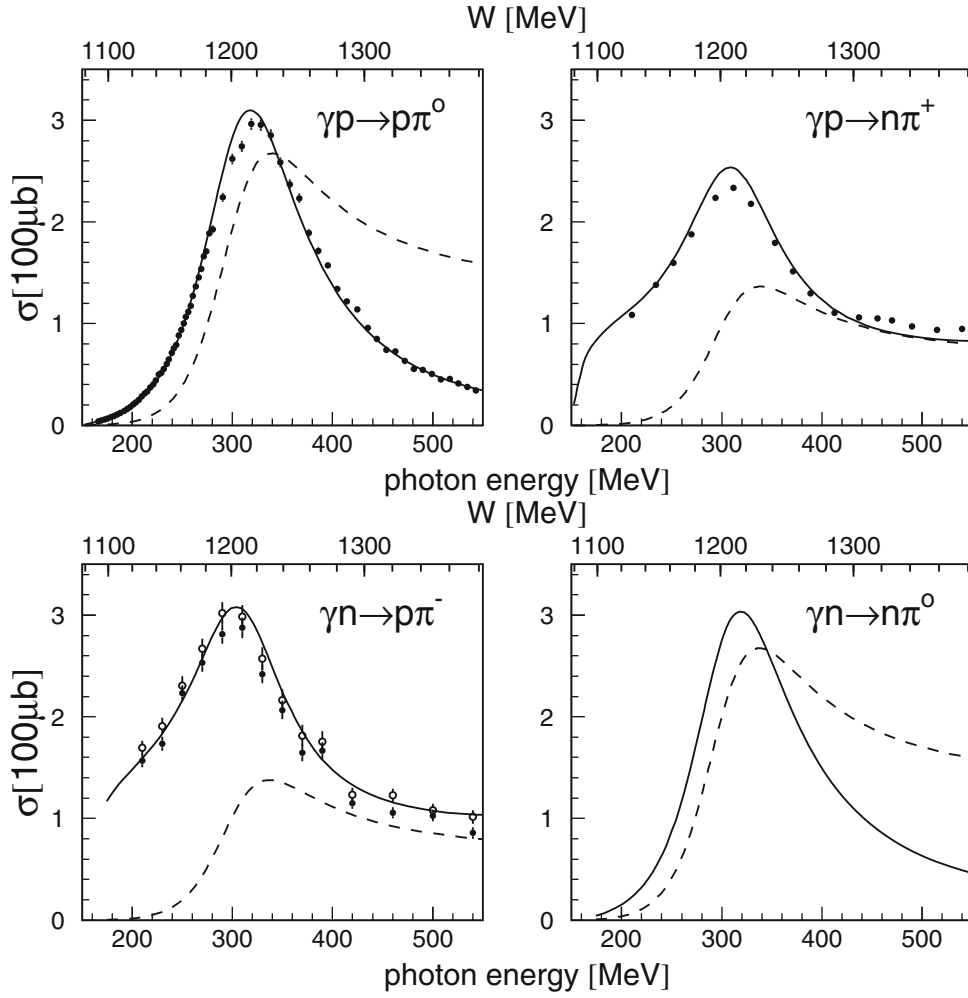
Fig. 5. Pion production in the Δ-resonance region. Data: $p\pi^0$ final state [38,39], $n\pi^+$ final state [40], $p\pi^-$ [36]. Curves: MAID-model [41], solid: full model, dashed: only $P_{33}(1232)$ resonance.

several overlapping $N^\star$ resonances where all three matrix elements contribute, such information is almost indispensable.

In general, the extraction of resonance properties from photoproduction reactions involving neutral mesons profits from the above discussed suppression of background terms. However, quasi-free measurements of neutral mesons off bound nucleons tend to suffer more strongly from FSI effects. Here, again pion production in the Δ region is a nice example. Figure 6 shows a few typical angular distributions for the $\gamma d \to \pi^- pp$ and $\gamma d \to \pi^0 np$ reactions close to the Δ-peak. For the π^0-channel only the breakup reaction is considered, coherent contributions to the $\pi^0 d$ final state are removed with kinematical cuts. The results are compared to a model calculation by Darwish, Arenövel, and Schwamb [42], which takes into account FSI effects in all two-body subsystems (although it turns out that only NN FSI is important). The large influence of FSI for the neutral final state is clearly visible. A major effect is that part of the reaction strength, in particular for pion forward angles for which the momentum mismatch between the two nucleons is smallest, is re-distributed to the
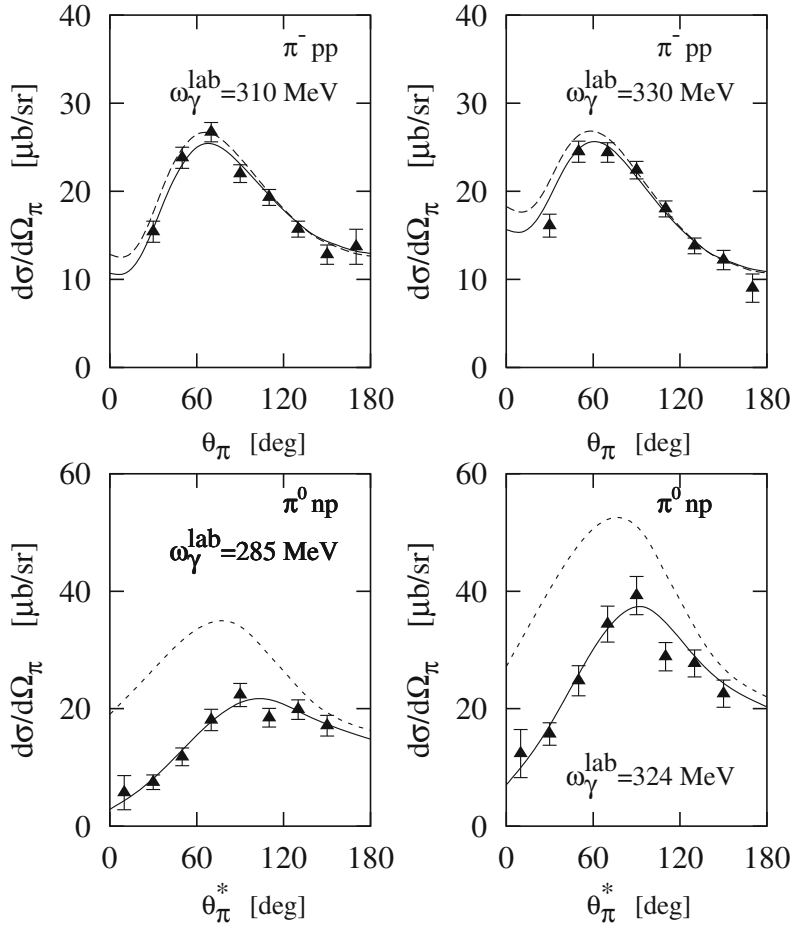
Fig. 6. Angular distributions [42] for the reactions $\gamma d \to \pi^- pp$ (data from [36]) and $\gamma d \to \pi^0 np$ (data from [39]) compared to model calculations from [42], solid: full model, dashed: without FSI.

coherent channel. As a consequence, the sum of breakup and coherent contributions is a much better estimate for the sum of the proton/neutron elementary cross sections than the quasi-free part (see [30] for details). Therefore, in this case a measurement of quasi-free cross sections in coincidence with recoil nucleons will produce model dependent results for the elementary cross sections. The inclusion of such strong FSI effects in the models is far from trivial, results for pion production from the work of Darwish et al. [42] are only available in the Δ resonance region. Recently, Tarasov et al. [43] have presented results for $\gamma n \to p\pi^-$ from the deuteron up to incident photon energies of 3 GeV, but comparable calculations for the $n\pi^0$ final state are still missing.

Photoproduction of neutral pions in the Δ-resonance region is of course quite well understood. But only a little bit higher in energy, in the second resonance peak built from the $P_{11}(1440)$, $D_{13}(1520)$, and $S_{11}(1535)$ resonances, photoproduction of neutral pions off the deuteron is not well understood. This is demonstrated in Fig. 7. The results for the reaction $\gamma p \to p\pi^0$ for the free proton are reproduced by the SAID partial wave analysis [35] and the MAID model [41] (which is not surprising because the results are input to the model analyses). But the Fermi smeared sum of neutron and proton cross sections, which agrees well with the data in the tail of the
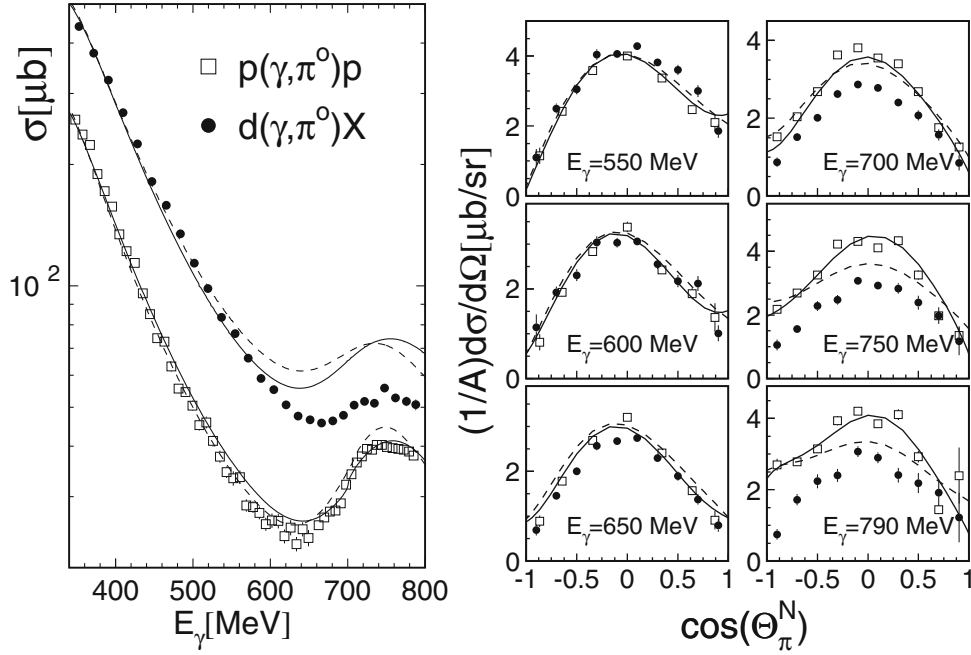
Fig. 7. Single π^0 photoproduction off the free proton and the deuteron in the second resonance region (note that $d(\gamma, \pi^0)X$ includes the $np\pi^0$ and $d\pi^0$ final states). Left hand side: total cross sections. Curves: results from the SAID analysis [35] (solid), and MAID-model [41] (dashed). For the deuteron from both models the sum of proton and neutron cross section folded with nuclear Fermi motion is taken. Right hand side: angular distributions, solid curves: SAID proton, dashed curves: Fermi smeared average of SAID proton and neutron.

Δ-resonance, significantly overestimates the second resonance peak. In the absence of detailed model calculations for FSI effects and without exclusive data in coincidence with recoil nucleons, it is impossible to decide whether this indicates a problem in the model predictions for the free $\gamma n \to n\pi^0$ reaction or nuclear effects. Exclusive data in coincidence with recoil nucleons could contribute a lot, because the comparison of the quasi-free cross section off the proton to (the Fermi smeared) free proton cross section would allow a test of FSI effects and such data would also allow a direct comparison of the neutron/proton ratio to model results (assuming that FSI effects are not strongly different for protons and neutrons).

The current experimental program for the investigation of the electromagnetic excitation spectrum of the neutron therefore aims at detailed measurements of the quasi-free cross section off nucleons bound in the deuteron for several different single $(\pi, \eta, \eta', \omega,...)$ and double $(\pi\pi, \pi\eta...)$ meson production channels. The comparison to other light target nuclei like ^{3}He, ^{4}He,... can add information about the importance of nuclear effects. This program will not only study differential cross sections but also single and double polarization observables.

1.2 Meson-nucleus interactions

The interaction of mesons with nuclei is a major source of information about the strong interaction. Elastic and inelastic reactions using secondary pion and kaon beams have revealed many details of the nucleon - meson potentials. However, secondary meson beams are only available for long-lived, charged mesons. Much less is

known for short-lived mesons like the η, η', and ω. Their interactions with nuclei can be studied only in indirect ways. The general idea is to produce them by some initial reaction in a nucleus and then study their interaction with the same nucleus.

In this section we will discuss three different lines of research for the interaction of mesons with nuclei: (1) The study of the scaling of nuclear production cross sections with mass number, shedding light on nuclear absorption probabilities, in-medium effects on meson-nucleon interaction probabilities, and meson in-medium widths, (2) the possible in-medium modification of the σ-meson related to partial restoration of chiral symmetry studied via double-meson production reactions, and (3) the search for the formation of mesic nuclei via coherent meson production reactions.

1.2.1 Meson absorption and in-medium widths

The study of the scaling of meson production cross sections with the nuclear mass number A is a basic type of experiment which typically exhibits a

$$\frac{d\sigma}{dT}(T) \propto A^{\alpha(T)}, \tag{3}$$

behavior, where T is the kinetic energy of the pions. A value of α close to unity corresponds to a cross section scaling with the volume of the nucleus, i.e. with vanishing absorption, while a value of $\approx 2/3$ indicates surface proportionality, corresponding to strong absorption. These scaling coefficients can then be converted to absorption cross sections using for example Glauber-type approximation models. Typical results for α as a function of T are shown in Fig. 8 for π^0 and η mesons. Pions show strong FSI at kinetic energies large enough to excite the $\Delta(1232)$, but are almost undisturbed for energies below the Δ excitation threshold. The situation is completely different for η-mesons, which show strong absorption for all kinetic energies measured so far. The reason is the overlap of the s-wave resonance $S_{11}(1535)$, which couples strongly to the $N\eta$-channel, with the production threshold. Eta-production in the threshold region is therefore completely dominated by this resonance [13]. The η-nucleon absorption cross section $\sigma_{\eta N}$ was determined from such data [45] to lie in the range of 30 mb, corresponding to a typical mean free path of $\lambda \approx 2$ fm.

A similar analysis is based on the so-called transparency ratio R, which compares the total production cross section $\sigma_{\gamma A \to VX}$ from a nucleus with mass number A to A-times the elementary production cross section $\sigma_{\gamma N \to VX}$ on the nucleon:

$$R = \frac{\sigma_{\gamma A \to VX}}{A\,\sigma_{\gamma N \to VX}}\,, \qquad\qquad R_A = \frac{12\cdot\sigma_{\gamma A \to VX}}{A\,\sigma_{\gamma C_{12} \to VX}} \tag{4}$$

where V denotes any meson. In order to account for the cross section difference between the proton and neutron and possible secondary production processes it is better to normalize to an average nucleon cross section measured for a light target nucleus with equal proton and neutron number (R_A defined in Eq. (4) for the reference nucleus ^{12}C). An example for such an analysis for the ω meson [47] is shown at the right hand side of Fig. 8 where the transparency ratios are compared to model calculations assuming different in-medium widths of the ω meson. As a result of the analysis, an in-medium width of the ω meson on the order of 130–150 MeV in normal nuclear matter has been found and, from a Glauber-type analysis, an absorption cross section of 70 mb was deduced. This value is roughly a factor of three larger than the input used for $\sigma_{\omega N}$ in the models. A similar result had been previously reported from the LEPS collaboration for the Φ meson [48]. In this case an absorption cross section of ≈ 30 mb was deduced, which has to be compared to the free nucleon absorption
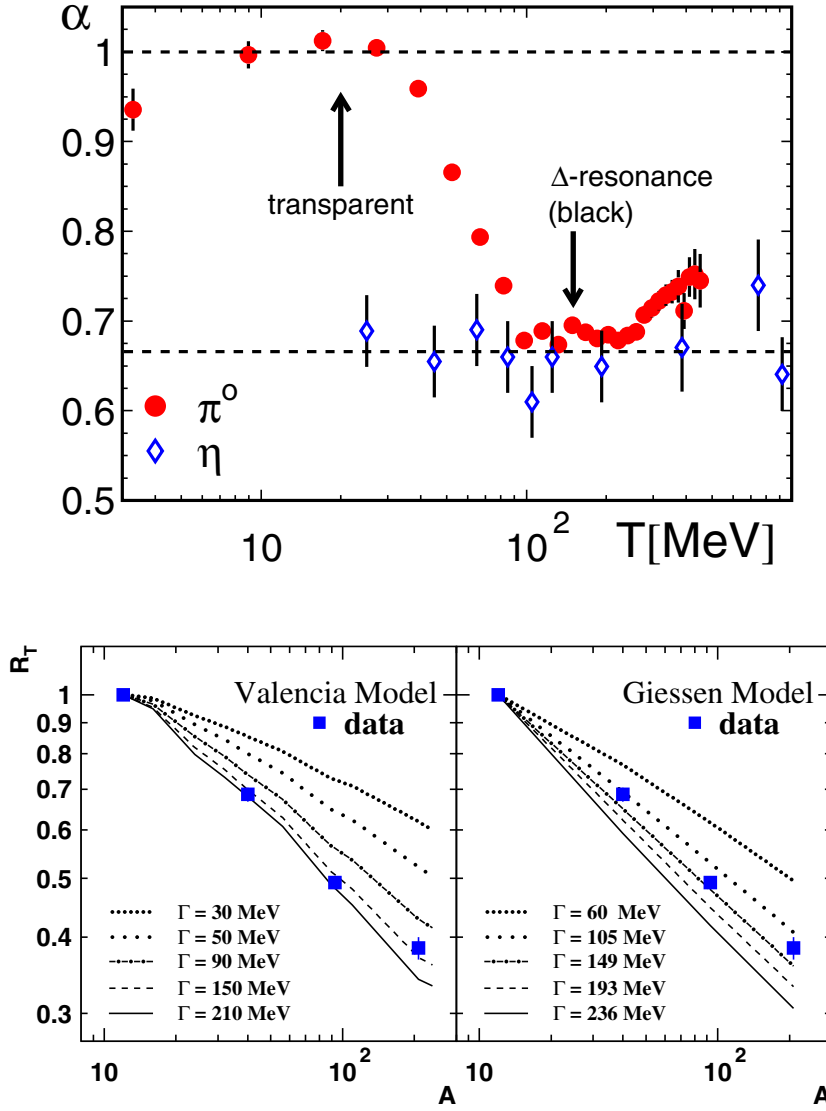
Fig. 8. Upper part: scaling parameter α as function of mesons kinetic energy for π^o [44] and η mesons [45,46]. Bottom part: analysis of the transparency ratio for photoproduction of ω-mesons [47].

cross section of 7.7–8.7 mb. Both experiments have produced strong evidence for the much discussed in-medium modification of vector mesons. A detailed review, including other related results for vector mesons, can be found in [1].

1.2.2 The σ-meson in matter and double-pion production

A particularly interesting prediction for in-medium effects for scalar mesons is the mass-split between the $J^\pi=0^-$ pion and its chiral partner, the $J^\pi=0^+$ σ-meson. Their masses are very different in vacuum, which is a well-known manifestation of chiral
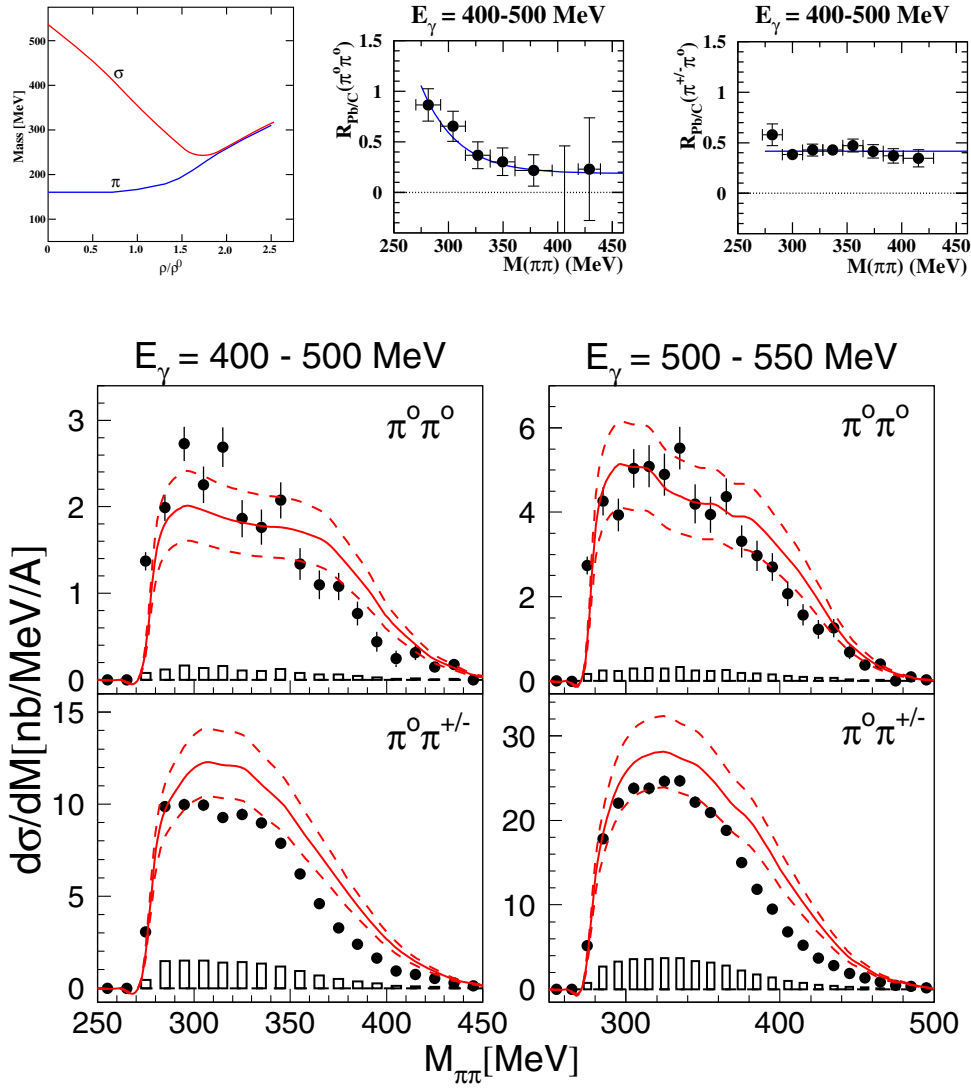
Fig. 9. Upper row, left hand side: predicted density dependence of π and σ mass [50], center and right: measured $R_{Pb/C}$ ratio for $\pi^o\pi^o$ and $\pi^{\pm}\pi^o$ [57]. Bottom row: pion-pion invariant mass distributions for ^{40}Ca [58] compared to results of the BUU model [49]. The bars at the bottom represent the systematic uncertainty of the data, the dashed lines represent the error band for the BUU calculation.

symmetry breaking. The naive assumption that the two masses should become degenerate in the chiral limit is supported by model calculations. A typical result is the density dependence of the mass calculated in the Nambu-Jona-Lasino model by Bernard, Meissner and Zahed [50] (see Fig. 9, left hand side). The σ-mass drops as a function of nuclear density. The predicted effect is already large for normal nuclear matter density ρ_o, where the pion mass is still stable. Since the σ meson couples strongly to scalar-isoscalar pion pairs the predicted effect should influence the invariant mass spectra of such pairs in the nuclear medium, producing a downward shift of the invariant-mass distributions of such pairs. This prediction has been

experimentally investigated with pion- and photon-induced double pion production reactions [51–58]. The CHAOS collaboration [51–55] reported a downward shift for $\pi^+\pi^-$ pairs with respect to $\pi^+\pi^+$ pairs from pion induced reactions. The Crystal Ball collaboration at BNL [56] observed a low-mass enhancement of strength for heavy nuclei in π^--induced $\pi^0\pi^0$ production. In photon-induced reactions, a downward shift of the invariant-mass distributions of $\pi^0\pi^0$ pairs with respect to $\pi^0\pi^\pm$ pairs has been measured by the TAPS collaboration [57]. This is particularly clearly seen in the normalized ratios of the invariant mass distributions defined by

$$R_{(Pb/C)}(\pi^o\pi^o) = \frac{d\sigma_{Pb}(\pi^0\pi^0)}{\sigma_{Pb}(\pi^0\pi^0)dM} \bigg/ \frac{d\sigma_C(\pi^0\pi^0)}{\sigma_C(\pi^0\pi^0)dM} \tag{5}$$

and analogously for $R_{(Pb/C)}(\pi^o\pi^\pm)$. The results are shown in Fig. 9. The ratio rises at small invariant masses for $\pi^0\pi^0$ pairs but not for $\pi^0\pi^\pm$ pairs, which do not couple to the σ. However, intricate final-state-interaction effects [49,58] complicate the interpretation of the results. This is shown at the right hand side of Fig. 9, where precise invariant mass distributions for ^{40}Ca [58] are compared to calculation in the framework of the Boltzmann-Uehling-Uhlenbeck (BUU) model [49]. The data have some excess strength for $\pi^0\pi^0$ at small invariant masses, but the model results show the same trend although they include only 'trivial' FSI effects but no σ-in-medium effects. In the model, the main effect arises from 'side-feeding'. Pions can undergo charge exchange scattering, re-distributing the strength between different isospin states. Since the elementary production cross section for double $\pi^0\pi^0$ pairs is much smaller than for double charged or mixed charge pairs (which are of comparable order) the main effect is a shift of strength from $\pi^0\pi^\pm$ to $\pi^0\pi^0$. Inelastic scattering of pions tends to reduce their kinetic energy, so that the pion pairs from 'side-feeding' in average have smaller invariant masses than those which have not undergone FSI. Therefore the net effect is an enhancement of $\pi^0\pi^0$ pairs at small invariant mass, just the same as predicted for the σ-in-medium effect. More detailed experiments trying to disentangle the different contributions are required. Preliminary results from the Crystal Ball experiment will be discussed below.

1.2.3 Mesic nuclei

A much discussed question is, whether the strong interaction allows the formation of quasi-bound meson-nucleus states. So far all known meson-nucleus bound states involve at least partly the electromagnetic interaction. Pionic atoms are well established. Also deeply bound pionic states have been reported [59], where the binding results from the superposition of the repulsive s-wave π^--nucleus interaction with the attractive Coulomb force. Neutral mesons could form quasi-bound states only via the strong interaction. The meson-nucleus interaction for slow pions is too weak to form such states (cf the weak FSI effects for low energy pions in Fig. 8). The possible formation of quasi-bound ω-nucleus states and their investigation via photon induced reactions has been discussed by Marco and Weise [60]. However, so far, no conclusive experimental results are available.

The most promising case is the η-meson with the strong s-wave coupling to the $S_{11}(1535)$ resonance. First hints for an attractive ηN s-wave interaction came from a coupled channel analysis of the ηN scattering length in 1985 by Bhalerao and Liu [61]. A short time later, Liu and Haider [62] suggested the possible formation of quasi-bound η - nucleus states for $A > 10$ nuclei. Experimental evidence has been sought in pion induced reactions [63,64], but those experiments did not produce conclusive evidence. More recently, Sokol and co-workers [65,66] claimed evidence for

the formation of η-mesic nuclei from bremsstrahlung induced reactions on ^{12}C

$$\gamma +^{12}\text{C} \rightarrow p(n) +_{\eta}^{11}\text{B}(_{\eta}^{11}\text{C}) \rightarrow \pi^+ + n + X \qquad (6)$$

where the $n\pi^+$ pairs were detected in the final state. The η-meson is produced in quasi-free kinematics on a nucleon (p,n) so that it is almost at rest in the residual $A = 11$ nucleus. If a quasi-bound state is produced, the η-meson can be re-captured by a nucleon into the S_{11} excitation, which may then decay into a pion-nucleon back-to-back pair. Sokol and Pavlyuchenko [66] claim an enhancement above background from quasi-free pion production for certain kinematic conditions.

After precise low-energy data for the photoproduction of η-mesons off the proton [14], deuteron [67–70] and helium nuclei [71,72] became available, refined model analyses of the scattering length were done by many groups (see [73] for a summary). The results for the imaginary part are rather stable and cluster between 0.2 fm and 0.3 fm. The more important real part, which decides about the formation of bound states, is still less constrained. It runs all the way from a negative value of -0.15 fm to numbers close to and even above $+1$ fm [73]. However, most of the more recent analyses prefer large values above 0.5 fm, which has raised discussions about very light mesic nuclei and prompted theoretical studies of the η-interaction with ^{2}H, ^{3}H, ^{3}He, and ^{4}He systems [74–83]

Experimental evidence for light η-mesic nuclei has mostly been searched in the threshold behavior of η-production reactions. The idea is that quasi-bound states in the vicinity of the production threshold will give rise to an enhancement of the cross section relative to the expectation for phase space behavior. Many hadron induced reactions have been studied in view of such effects in particular: $pp \rightarrow pp\eta$ [84–86], $np \rightarrow d\eta$ [87,88], $pd \rightarrow \eta^3$He [89], $dp \rightarrow \eta^3$He [90–92], $\boldsymbol{d}d \rightarrow \eta^4$He [93], and $pd \rightarrow pd\eta$ [95]. In particular the $pd \rightarrow \eta^3$He [89] and $dp \rightarrow \eta^3$He reactions [90–92] show an extremely steep rise at threshold, implying a very large η^3He scattering length.

If such states do exist, they should show up independently of the initial state of the reaction. Threshold photoproduction of η-mesons from light nuclei is a clean tool for such experiments, but for that the η-mesons have to be produced coherently off the target nuclei. Since threshold photoproduction of the η is dominated by an isovector spin-flip amplitude exciting the $S_{11}(1535)$ (see [30] for a summary) the coherent cross section is very small for the isoscalar deuteron and practically forbidden for the isoscalar scalar ^{4}He nucleus. Only the $I = 1/2$, $J = 1/2$ ^{3}H and ^{3}He nuclei have reasonably large cross sections for $\gamma A \rightarrow A\eta$.

The ^{3}He system has been investigated with photon induced reactions by Pfeiffer et al. [96]. Possible evidence for the formation of a quasi-bound state was reported from the behavior of two different reactions. The coherent η-photoproduction γ^3He $\rightarrow \eta^3$He showed a strong threshold enhancement with angular distributions much more isotropic in the threshold region than expected from the nuclear form factor. Both are indications at least for strong FSI processes. Furthermore, in an approach similar to the Sokol experiment [66], the excitation function for π^0-proton pairs was investigated. After background subtraction, it showed a slight enhancement at the η-production threshold for pairs emitted back-to-back in the γ^3He cm-system. Preliminary results from a follow-up experiment with much better statistical quality will be discussed below.

2 Experimental facilities

In this section we will give a short overview of the main facilities involved in the study of photoproduction from nuclear targets. All experiments are based at electron accelerators equipped with tagged photon beams, based on the bremsstrahlung technique
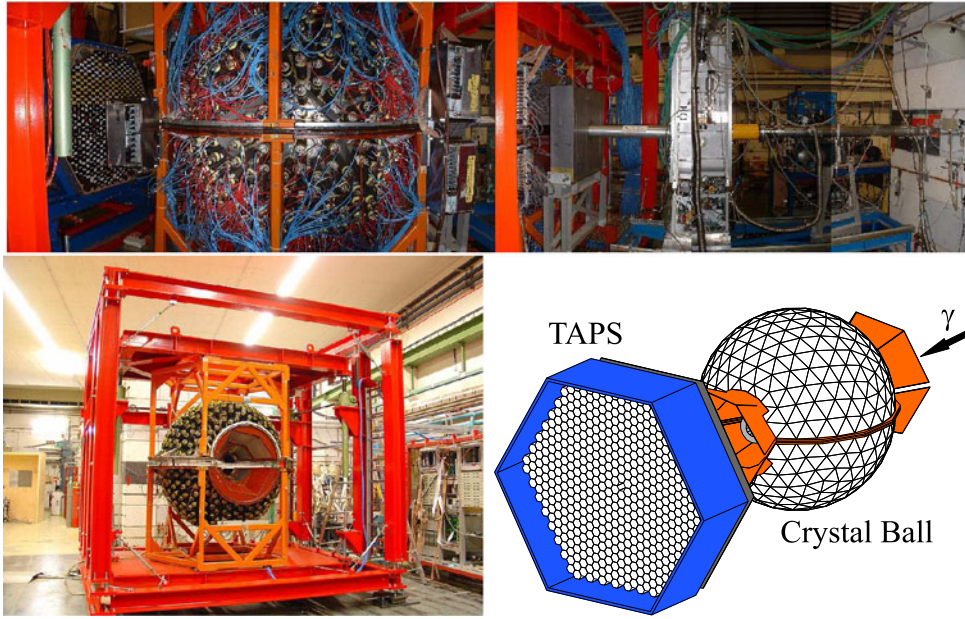
Fig. 10. Overview of the MAMI setup. Upper part: beam coming from the right, Crystal Ball at the left of the picture, TAPS forward wall at the very left. Bottom part, left hand side: Crystal Ball in setup phase, right hand side: schematic drawing of the calorimeter.

or Laser-backscattering. Most of them can be linearly and/or circularly polarized. The additional availability of polarized protons and deuterons, using frozen-spin butanol or HD targets, allows the study of a full set of single and double polarization observables for meson production reactions off the proton and the neutron. Since the detector systems at these facilities are optimized for different reaction types involving different particles mostly from photoproduction off the free proton, they are more or less well adapted for measurements off quasi-free neutrons. While some of them (in particular the 4π electromagnetic calorimeters) can easily measure even all-neutral multiple-meson final states like $\pi^0\pi^0 n$, $\pi^0\eta n$, devices relying more or less on magnetic spectrometers need at least some charged particles in the final state and sometimes cannot detect the recoil neutrons.

2.1 The Crystal Ball/TAPS setup at the Mainz MAMI accelerator

The MAMI accelerator in Mainz [97,98] now delivers electron beams with energies up to 1.5 GeV, typical longitudinal polarization of the beam reaches values above 80% and is very stable. Photon beams are produced by the bremsstrahlung process and are tagged with the Glasgow magnetic spectrometer [99]; at maximum electron energy with a typical resolution of 4 MeV. Linearly polarized photon beams are produced using coherent bremsstrahlung from diamond lattices. Since the accelerator is designed also for electron scattering experiments, it can deliver electron beam intensities far larger than needed for tagged photon experiments ($\approx 100\,\mu$A, compared to some tens of nA used for tagging). Liquid hydrogen, liquid deuterium, liquid ^{3,4}He, gaseous polarized ^{3}He, frozen-spin butanol (polarized protons), frozen-spin deuterated butanol (polarized deuterons), and solid targets can be and have been used at
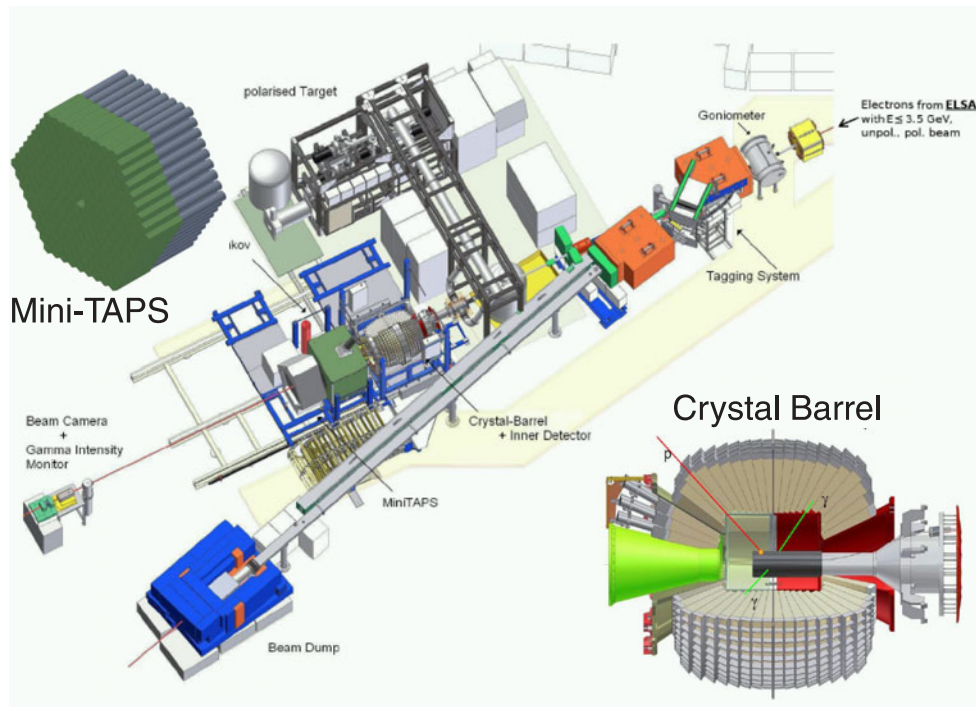
Fig. 11. Experimental setup at the Bonn ELSA accelerator combining the Crystal Barrel detector, part of the TAPS detector as forward wall, inner detectors, the photon tagging facility and the frozen-spin polarized target.

this facility. The typical detector equipment is summarized in Fig. 10. A 4π electromagnetic calorimeter has been set up, combining the Crystal Ball detector [100] (672 NaI crystals covering the full azimuthal angle for polar angles from $20°$ to $160°$) with 384 BaF_2 crystals from the TAPS detector [101,102], configured as a forward wall. The forward wall is mounted 1.475 m downstream from the target and covers polar angles from $\approx 2°$ to $21°$. The Crystal Ball is equipped with an additional **P**article **I**dentification **D**etector (PID) [103] and cylindrical multiple wire chambers surrounding the target and all modules of the TAPS detector are capped with individual plastic scintillators for charged particle detection. This setup, and earlier simpler detector configurations based on the TAPS detector or the GDH-experiment, have been used to study photoproduction off nuclei from the deuteron to the most heavy targets. Currently, measurements of double polarization observables for meson photoproduction off the proton and the neutron are under way.

2.2 The Crystal Barrel/TAPS setup at the Bonn ELSA accelerator

The electron stretcher accelerator facility ELSA [104,105] delivers electron beams with energies up to 3.5 GeV. The intensity is lower (typically a few nA) than for MAMI. Circularly or linearly (see [106] for details) polarized beams are produced using the same techniques as at MAMI and a polarized frozen-spin butanol target, very similar to the one used at MAMI, is available. The whole setup is summarized in Fig. 11. The main detector is again a 4π electromagnetic calorimeter combining the Crystal Barrel detector [107] (1290 CsI (Tl) crystals of 16 radiation lengths X_o

all mounted in a target pointing geometry) with part of the TAPS detector (216 BaF_2 crystals) as forward wall ('Mini-TAPS'). In this case only 'Mini-TAPS' and the most forward part of the Barrel (90 CsI modules) are read out with photomultipliers. The rest of the Barrel is read with photodiodes, so that it does not deliver timing information and cannot be used in the first level trigger. This is not a significant disadvantage for measurements off the free proton, where in addition to hits in the forward part of the calorimeter the proton can generate triggers in the 'Inner-detector' [108], a three-layer scintillating fiber detector around the target, covering polar angles between $28°$ and $172°$. It limits, however, the type of reactions that can be studied off quasi-free neutrons to reactions with large photon multiplicity, which have reasonable trigger efficiencies from the forward part of the detector. Therefore, so far in particular channels like $\eta \to 3\pi^0 \to 6\gamma$ [46,109], $\eta' \to \pi^0\pi^0\eta \to 6\gamma$ [110], $\omega \to \pi^0\gamma \to 3\gamma$ [47,111–113], $\pi^0\pi^0 \to 4\gamma$ [114], and $\pi^0\eta \to 4\gamma$ [115] with three to six photons in the final state have been studied for nuclear targets. It is, however, planned to upgrade the trigger capability of the detector by a new readout system based on **A**valanche **P**hoto**D**iodes (APDs), which can deliver time information and trigger signals. Also at this facility a large program to measure single and double polarization observables off the free proton and the quasi-free neutron is under way.

2.3 The CLAS detector at JLAB

The CEBAF Large Acceptance spectrometer (CLAS) [116] is housed in Hall B of the Thomas Jefferson National Accelerator Facility in Newport News. The detector is installed at a beam line which can deliver electron beams from $0.8\,\text{GeV}$ to $6\,\text{GeV}$ which may be polarized (polarization degrees up to 85%). The photon tagging system can tag photons in the range from 20% to 95% of the incident electron energy (for electron energies up to $6.1\,\text{GeV}$). Circularly polarized photon beams are produced as usual with longitudinally polarized electron beams and coherent bremsstrahlung from a diamond is used to obtain linearly polarized beams. A butanol cryo-target of the frozen-spin type is available for polarized protons and deuterons. The core of the detector is a toroidal magnet built from six superconducting coils, symmetrically arranged around the beam line. All six sectors are equipped with 34 layers of tracking chambers. This setup allows the full reconstruction of the three-momentum of charged particles with high resolution. The tracking region is surrounded by plastic scintillators. Charged hadrons are identified by combining the momentum, time-of-flight, and path length information. In addition, for polar angles smaller than $70°$, photons and neutrons can be detected in an electromagnetic calorimeter. The detector is often operated in the missing mass mode, i.e. all particles except one are detected and the mass of the only missing particle is than reconstructed from the reaction kinematics. In that way, all kinds of single meson production reactions off free protons can be studied over a large range of incident photon energies. This technique does not work for multiple production of neutral mesons ($\pi^0\pi^0$, $\pi^0\eta$) or for photoproduction of neutral mesons off the neutron (unless the neutral mesons decay into long-lived charged mesons like $K^0 \to \pi^+\pi^-$). Therefore, the programs aiming at the study of meson photoproduction off neutrons at MAMI and ELSA on one side and at CLAS on the other side, are nicely complementary. The CLAS experiment is ideal for reactions with high charged particle multiplicity in the final state like $\gamma n \to p\pi^-$ [37], or $\gamma n \to K^0\Lambda \to (\pi^+\pi^-)(\pi^- p)$, while the 4π electromagnetic calorimeters are in advantage for the 'all neutral' final states.

Apart from the measurement of angular distributions and polarization observables for meson photon production off quasi-free neutrons, the CLAS experiment has also contributed to the investigation of meson in-medium properties via a study of the

$\gamma A \rightarrow e^+e^- X$ reaction [117,118]. The ρ, ω, and ϕ vector mesons have small branching ratios (order of 10^{-5} to 10^{-4}) into the e^+e^- channel and can be reconstructed from the invariant mass of the lepton pairs. The advantage of this type of experiment is that, both in the initial and final state, only electromagnetic interaction contributes, so that initial and final state interaction effects are minimized. Due to kinematical limitations only vector mesons with momenta above 1 GeV could be detected, so that the longer-lived ω and ϕ mesons decayed mostly outside the nuclei without significant in-medium modifications. The short-lived ρ in turn showed a clear collisional broadening of its width by roughly 70 MeV, but no shift of its mass.

2.4 The GeV-γ experiment at LNS at Tohoku University

The third facility that uses a tagged bremsstrahlung beam is located at the Laboratory of Nuclear Science (LNS) at Tohoku University in Sendai, Japan. The primary electron beam with energies up to 1.2 GeV is produced by a synchrotron (Stretcher Booster Ring (STB)) [119]. The tagging system is described in detail in [120]. The system uses one of the magnets from the synchrotron (a C-shaped sector magnet) as magnetic spectrometer for photon tagging. The bremsstrahlung target is a thin carbon fiber string (diameter of $11\,\mu$m), which can be moved step-wise into the internal beam to produce the desired intensity of bremsstrahlung photons (typical intensities between $3 \times 10^6\,\mathrm{s}^{-1}$ and $2 \times 10^7\,\mathrm{s}^{-1}$). The tagging counters are two rows of plastic scintillators. The first row consists of 50 counters with a width of 5 mm, which corresponds to an energy bin width of 6 MeV at $E_\gamma = 1$ GeV. The second row of scintillators has larger width, each module covering four modules of the first row (except that at highest energies which covers six modules) and reduces the background via a coincidence condition.

The experimental setup for the detection of photons is described in [142]. The main component are four blocks of in total 206 CsI detectors. The two forward blocks of 124 modules each cover polar angles from 15° to 72° and azimuthal angles from −17° to 17° and the two backward blocks of 29 modules each cover polar angles of 95° to 125° at azimuthal angles of −12° to 12°. Plastic scintillators in front of the CsI modules are used for charged particle identification. The coverage of the solid angle was thus far below 4π. More recently, a new detector setup, the electromagnetic calorimeter FOREST [122], has been installed at LNS. It combines three electromagnetic calorimeters of CsI modules, Lead/SciFi blocks, and Lead Glass Čerenkov counters, covering roughly 90% of 4π.

For photoproduction reactions off the free proton or quasi-free nucleons from the deuteron solid hydrogen or deuterium targets are used. Polarization observables cannot be investigated.

This experiment has been for example used for the study of η photoproduction off the free proton [142], quasi-free of the deuteron [130], and also off heavy nuclei [121]. Due to the low acceptance and low detection efficiency for recoil nucleons, the experiments off the nuclei supplied only the inclusive cross section without detection of coincident recoil nucleons. The quasi-free neutron cross section was extracted by subtracting the free-proton cross section (after folding with the momentum distribution of protons bound in the deuteron) from the inclusive deuteron data.

2.5 The LEPS facility at SPring-8 in Osaka

The last two facilities are based on a different technique for the production of tagged photon beams, namely the backscattering of laser light from high energy electrons. A

certain advantage of this type of experiment is that linearly and circularly polarized beams can be easily produced by using correspondingly polarized laser light. The polarization characteristics are different from the bremsstrahlung technique, in particular for linearly polarized photons. The latter produces polarization in the coherent peaks of the bremsstrahlung spectrum; reasonable polarization degrees can only be obtained for photon energies up to 50% of the electron beam energy. Beams from laser backscattering reach the maximum polarization degree at maximum photon beam energies.

The **L**aser-**E**lectron **P**hoton beam line (LEPS) experiment is located at the 8-GeV storage ring of the **S**uper **P**hoton **ring** (SPring-8). The setup is described in [123]. Laser light from an Ar-ion laser (wavelengths between 333.6 and 363.8 nm) is reflected into the electron beam line in a straight section. The photons backscattered from the 8 GeV electrons reach maximum energies of 2.4 GeV. The scattered electrons are momentum analyzed by the last bending magnet before the straight section of the beam line and then detected in a tagging counter. The tagging detector combines two layers of scintillator hodoscopes with two layers of silicon strip detectors. The scintillators of both hodoscopes are 5 mm wide and arranged with 2.2 mm overlap. The hodoscopes reject accidental background and the hit position on the strip detectors (strip width 0.1 mm) defines the energy of the scattered electrons. The typical energy resolution is in the range of 15 MeV.

The LEPS detector system is quite different from the more-or-less 4π covering electromagnetic calorimeters discussed above or the large angle magnetic spectrometer CLAS. It is optimized for the detection of forward-going charged hadrons. The two main components of the device are a dipole magnet at forward angles covering ±0.4 rad in the horizontal and ±0.2 rad in the vertical direction. Charged particles deflected by the magnetic field are detected in a time-of-flight wall made of 40 plastic scintillators each of 12 cm widths, 4 cm thickness and 200 cm length mounted with an overlap of 1 cm. The start signal for the time-of-flight measurement is provided by the RF of the electron ring. The system is equipped with a start detector (for trigger purposes) and a Čerenkov Aerogel counter for the rejection of electromagnetic background, both mounted in front of the magnet entrance. A silicon vertex detector also in front of the magnet entrance and three multiple-wire drift chambers, one downstream and two upstream of the magnet, are used for track reconstruction of charged particles.

This setup is particularly well suited to study strangeness production via the spectroscopy of forward going charged kaons (see e.g. [123]). It has significantly contributed to the study of the in-medium properties of vector mesons with the measurements of transparency ratios for the photoproduction of ϕ mesons off nuclei, where it found a substantial increase of the in-medium ϕN absorption cross section with respect to the ϕN absorption in free space. It was also strongly involved in experiments reporting tentative evidence for the observation of pentaquark states in the $\gamma n \to K^+ K^- n$ reaction using carbon targets [124], which are, however, heavily disputed.

2.6 The GRAAL facility at ESRF in Grenoble

This overview would be incomplete without a short discussion of the **GR**enoble **A**nneau **A**ccelerateur **L**aser (GRAAL) at the **E**uropean **S**ynchrotron **R**adiation **F**acility (ESRF) in Grenoble, although this experiment has been shut-down recently.

The photon beam was produced similarly to the LEPS experiment by shining a laser on the 6 GeV electron beam of the synchrotron. Depending on the wavelength of the laser, Compton-edges at 1.1, 1.4, 1.47, and 1.53 GeV have been produced. An

overview over the beam-line setup and tagger device is e.g. given in [125]. Also in this setup one of the synchrotron bending magnets was used for the deflection of the backscattered electrons, which were then detected in a silicon microstrip detector (128 strips with a pitch of $300\,\mu$m). Typical resolution for the photon beam energy was 16 MeV (FWHM). Polarized beams were produced by the use of polarized laser light. Polarized targets were not used.

The detection system **L**arge **A**cceptance **GR**aal-beam **A**pparatus (for) **N**uclear **G**amma **E**xperiments (LAγRANGE) combined two main components [125]. The target was surrounded by a BGO electromagnetic calorimeter consisting of 488 crystals, 21 radiation lengths long, which covered polar angles from $25°$ to $155°$ for the full azimuthal angular range. Two cylindrical wire chambers and a barrel of plastic scintillators in the BGO ball allowed the reconstruction of position and energy loss of charged particles. The position of charged particles at forward angles up to $25°$ was measured by two planar wire chambers and the energy was derived from a time-of-flight measurement by a hodoscope of plastic scintillators placed 3 m away from the target. Photons and neutrons at forward angles could be detected in a lead-scintillator sandwich wall behind the plastic hodoscope.

During the last few years, this experiment produced significant results for meson photoproduction reactions of the quasi-free neutron bound in the deuteron, among them the first measurement of the beam asymmetry Σ for η photoproduction of the neutron [126], a measurement of total cross sections, invariant mass distributions, and beam asymmetries for double π^0 production off the neutron [177], and the first experimental evidence for the narrow structure observed recently in the excitation function of η photoproduction off the neutron [148].

In the meantime, the experiment has been dismounted and the BGO ball is now being installed at the Bonn ELSA accelerator in a new setup, combining it with a forward magnetic spectrometer.

3 Analysis methods

The measurement of meson production reactions off the neutron via quasi-free reactions off bound neutrons requires in general the detection of the participant neutron. This can be done with different techniques, electromagnetic calorimeters like the Crystal Ball (NaI scintillators), Crystal Barrel (CsI scintillators), or TAPS (BaF$_2$ scintillators) are also capable of neutron detection, although with limited detection efficiency (typically on the 15% - 30% level) and without any energy resolution. Kinetic energies of the recoil neutrons can be measured via time-of-flight provided the target - detector distance is large enough, which is the case for the TAPS forward walls at MAMI and ELSA and was the case for the time-of-flight forward walls of the GRAAL experiment. But this covers only the forward range of the recoil neutrons, corresponding to backward angles of the produced mesons. Alternatively, as discussed below, the kinetic energy may be reconstructed from the reaction kinematics. Detection efficiencies for the neutrons must either be simulated with Monte Carlo programs or can be measured with reactions where direction and kinetic energy of the neutrons can be reconstructed from the reaction kinematics (e.g. from reactions like $\gamma p \to n\pi^+$ or $\gamma p \to n\pi^0\pi^+$), where the mesons are detected. The simulation of the neutron detection efficiencies is notoriously difficult and must always be cross-checked with experimental results. Nevertheless, as discussed in detail in [127] the use of the GCALOR program package [128] provides rather satisfactory results.

Fortunately, at least for some of the experiments, detection efficiency related problems can be tracked in a simple way. The cross sections for meson production off the
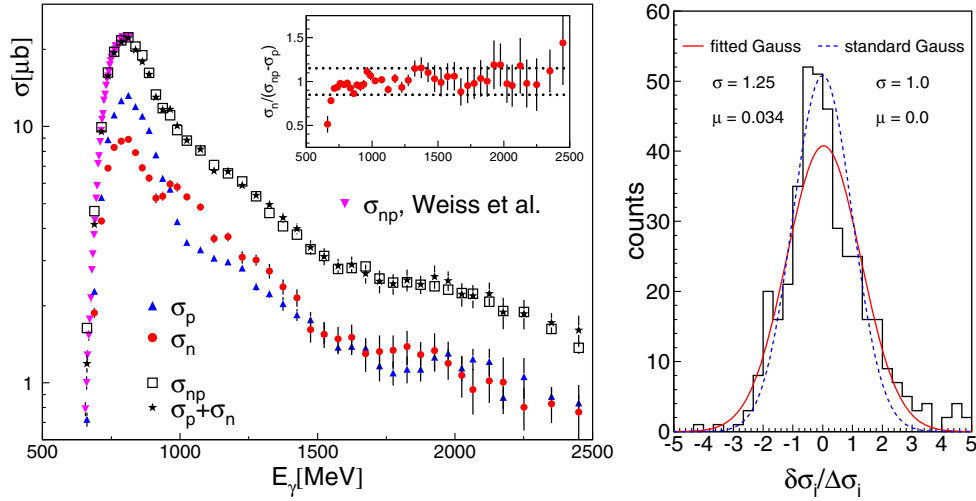
Fig. 12. Comparison of cross sections for quasi-free η photoproduction [127]. Left hand side: total cross sections, (Blue) upward triangles: quasi-free proton cross section σ_p, (red) dots: quasi-free neutron cross section σ_n, (black) open squares: inclusive quasi-free cross section σ_{np}, (black) stars: $\sigma_n + \sigma_p$. Downward (magenta) triangles: inclusive quasi-free cross section from Weiss et al. [70]. Insert: ratio of neutron cross sections. Right hand side: distribution of deviations between $d\sigma_n/d\Omega$ and $d\sigma'_n/d\Omega = d\sigma_{incl}/d\Omega - d\sigma_p/d\Omega$. Solid (red) curve: fitted Gaussian distribution (width $\sigma = 1.25$, mean $\mu = 0.034$), dashed (blue) curve: standard Gauss: ($\sigma = 1$, $\mu = 0$).

deuteron (or other light nuclei) must obey the relation:

$$\sigma_{incl} = \sigma_p + \sigma_n + \sigma_{coh}, \tag{7}$$

where σ_{incl} is the inclusive cross section without any condition for recoil baryons, σ_p, σ_n are the cross sections in coincidence with recoil protons and neutrons, and σ_{coh} is the coherent production cross section of the respective nucleus. As an example we discuss the photoproduction of η-mesons off the deuteron. In this case, (as in many others) the coherent production cross section σ_{coh} is negligible, so that the quasi-free neutron and proton cross sections must add up to the inclusive cross section. Only the detection efficiency of the η-meson enters into the inclusive cross section (where events with and without recoil nucleons are excepted). The completely different proton and neutron detection efficiencies enter into σ_p and σ_n so that Eq. (7) in general holds only when all detection efficiencies are correct. This means that the neutron cross section can be measured in two different ways, either as σ_n by the detection of recoil neutrons or as difference $\sigma_{n'} = \sigma_{incl} - \sigma_p$. The result of such an analysis from the Crystal Barrel/TAPS experiment [127] is shown in Fig. 12. The left hand side of the figure demonstrates the agreement of the total cross sections; the sum of quasi-free proton and neutron cross section agrees with the independently constructed inclusive cross section, and correspondingly the ratio of the neutron cross sections σ_n, $\sigma_{n'}$ is close to unity (see insert of Fig. 12, left hand side).

As a further test (cf Fig. 12, right hand side) the distribution of the deviations $\delta\sigma_i$ normalized by the statistical uncertainties $\Delta\sigma_i$

$$\frac{\delta\sigma_i}{\Delta\sigma_i} \equiv \frac{d\sigma'_n/d\Omega - d\sigma_n/d\Omega}{\sqrt{\Delta^2(d\sigma'_n/d\Omega) + \Delta^2(d\sigma_n/d\Omega)}} \tag{8}$$
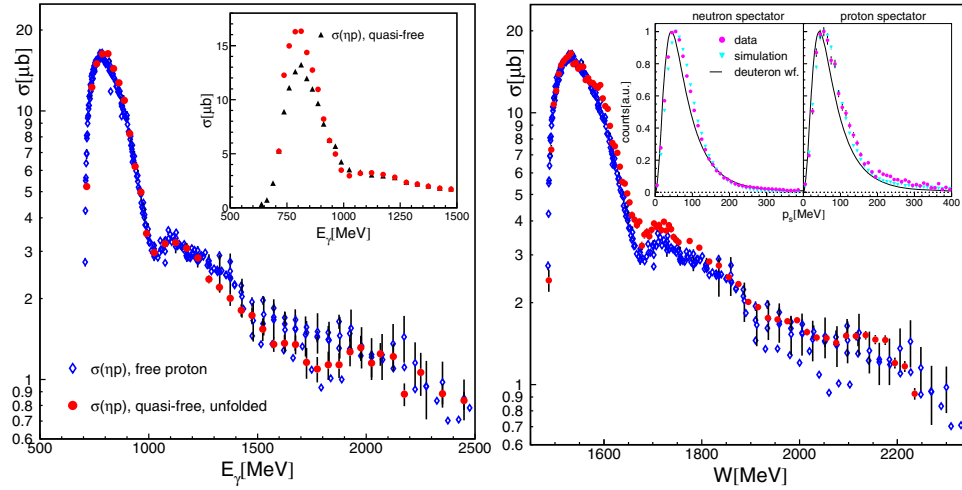
Fig. 13. Comparison of free and quasi-free photoproduction of η-mesons off the proton (see text). Left hand side: (blue) diamonds world data base for $\gamma p \to p\eta$ versus incident photon energy. (Red) dots: quasi-free $\gamma' p' \to' p'\eta$ reaction after applying correction factors for Fermi smearing. Insert: quasi-free data with (red dots) and without (black triangles) correction for Fermi motion. Right hand side: free proton data (blue diamonds) versus W. (Red) dots: quasi-free data from kinematical reconstruction of W. Insert: reconstructed momenta of spectator nucleons compared to momentum distributions from deuteron wave function (neutron spectator corresponds to detection of recoil proton and vice versa).

for all data points (420 entries) of the angular distributions from production threshold to 2.5 GeV is compared to a Gaussian distribution. The fitted Gaussian distribution corresponds to a width of $\sigma = (1.25 \pm 0.10)$ and a mean of $\mu = (0.034 \pm 0.110)$, fairly close to a standard Gaussian distribution. In particular, the mean is not significantly different from zero so that no indication for a systematic deviation is indicated. This test provides stringent limitations for systematic uncertainties related to the detection of the recoil nucleons. In case of the Crystal Barrel and Crystal Ball experiments, it has become a standard procedure. Some other experiments, like for example LNS at Tohoku do not measure the recoil neutrons and rely completely on $\sigma_{n'}$ constructed from inclusive deuteron and free (Fermi smeared) proton data (see e.g. [130]).

The more important problem related to the use of the deuteron or other light nuclei as target is the influence of nuclear effects, which may modify the elementary cross sections. The always present trivial effect from nuclear Fermi motion is quite well understood and, as discussed below, can be reliably accounted for. In the most simple approach, the results from model calculations can be folded with the momentum distribution of the bound nucleons before comparison to the data. In a somewhat more involved procedure discussed below, in many cases it is also possible, to correct the effects in the data.

Much more difficult are nuclear FSI effects etc., which are not very well understood in models, and may have a very different influence on different reaction channels. However, one can always cross-check the importance of such effects by a comparison of free proton data to the quasi-free proton data extracted from nuclear targets, taking into account the effects of nuclear Fermi motion. As an example, we discuss again η-photoproduction, but other reactions, even with very small cross sections, like Compton scattering [129], have been also studied in this way.

A comparison of free and quasi-free proton data is shown in Fig. 13. The figure on the right hand side shows a comparison of the world data base for the total cross section off the free proton to quasi-free proton data corrected for Fermi motion. In this case the correction was done by folding the free proton data with the Fermi motion, calculating as function of incident photon energy a correction factor from the ratio of unfolded to folded cross section and applying these factors to the quasi-free data (alternatively one could of course also compare directly the folded free-proton data to the quasi-free data). The agreement between the two data sets is quite good, demonstrating that nuclear effects beyond Fermi motion are not important in this case. The insert of the figure shows the effect of the Fermi smearing, which is of course particularly important in the steep slopes of the cross sections.

The above method does not assist in the extraction of an approximation of the free neutron cross section from quasi-free neutron data. In this case, the correction factors are unknown and one could only try to compute them in an iterative way, but this will converge only as long as no narrow structures or steep slopes are involved. However, there is an alternative possibility. Instead of analyzing the cross section as function of E_γ (or W computed from E_γ) one can directly compute the W of the system decaying into $N\eta$ from the four-vectors of the η and the recoil nucleon. In this way, the influence of Fermi motion is completely removed, at the price, that the experimental resolution for the four-vectors enters into W. The result of such an analysis for η-production off the proton is shown on the right hand side of Fig. 13. Again, free proton data and reconstructed quasi-free data are in very good agreement.

Applying this method to neutron data involves the technical problem of measuring the neutron four-vectors with good resolution. The high granularity of the 4π calorimeters provides good resolution for the direction of the neutron. However, the kinetic energy cannot be reconstructed from the deposited energy and the use of time-of-flight methods is restricted to the solid angle covered by the forward wall detectors (typically $20°$ of polar angle) since for the other detectors the time-of-flight path is too short. However, in the case of a deuteron target, a direct measurement of the neutron kinetic energy in not necessary; it can be reconstructed from the reaction kinematics. All kinematical observables of the initial state (photon and deuteron) are known. In the final state, the mass of all particles is known and the three-momentum of the meson is measured. When in addition the direction of the participant nucleon is measured, only four kinematical observables are missing: the kinetic energy of the participant nucleon and the three-momentum of the spectator nucleon. Since energy and momentum conservation give four independent constraints, the system is completely determined. The insert of Fig. 13 shows the momentum distributions of the undetected spectator nucleons constructed this way. They are compared to the momentum distribution predicted by the deuteron wave function, which, after taking care of detector resolution effects with a Monte Carlo simulation, agrees very well with the data. With this method one can in addition, via cuts on the spectator momentum, remove those events which are not close to quasi-free reaction kinematics and might suffer from stronger off-shell effects.

4 Final and preliminary results

In this section we will summarize new results from the ELSA and MAMI experiments, which have just been published, are in press, or in an almost final state of analysis.
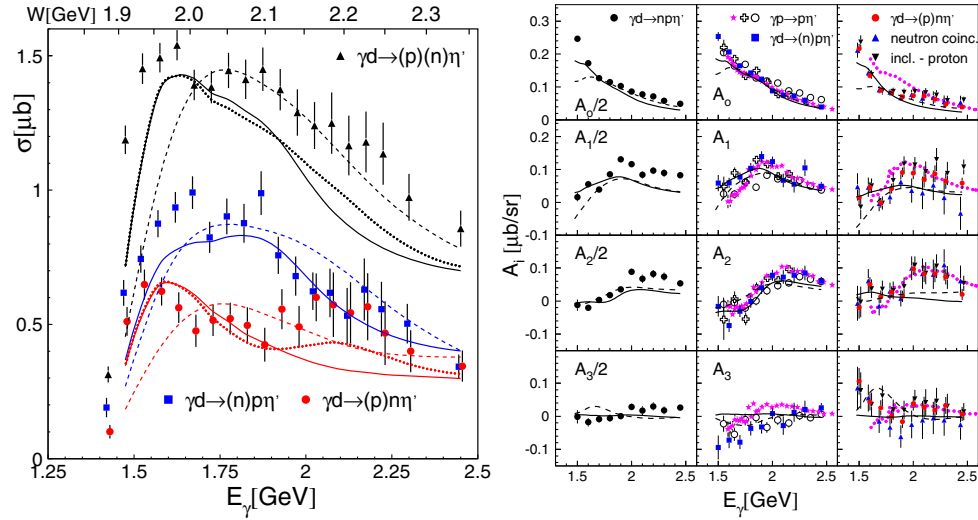
Fig. 14. Left hand side: total cross section for η' production off the deuteron [110]. Curves: fits with reaction models model, solid, dotted: different solutions from [131], dashed: η'-MAID [132]. Right hand side: coefficients of the Legendre Polynomials for the fitted angular distributions [110]. Left hand column: inclusive reaction scaled down by factor of 2. Center column (proton targets): quasi-free data (blue squares); free proton data: open crosses [133], open circles [17], (magenta) stars [16]. Right hand column (quasi-free neutron data): (blue) upward triangles from neutron coincidence, (black) downward triangles from difference of inclusive and proton data, (red) circles from averaged data. In all plots solid lines: NH model, dashed lines: η'-MAID; for neutron: (magenta) dotted lines CLAS proton data.

4.1 Meson photoproduction off the neutron − the η' meson

Photoproduction of η' mesons has recently attracted quite some interest. Due to its large mass of 958 MeV the production threshold on the free nucleon lies at 1447 MeV, corresponding to $W \approx 1896$ MeV. This is a range where many hitherto unknown N* resonances are predicted by quark models. Like the η, the isoscalar η' can only be emitted by N* states and close to threshold only a few partial waves contribute.

Rather precise data off the free proton have been measured by the CLAS experiment [16,133] and at ELSA [17]. Unfortunately, it turned out [131] that in this case even close to threshold differential cross section data alone cannot fix the model parameters. Although most analyses agree on a strong contribution from a S$_{11}$ resonance, the position, width, and coupling strength of this state are not well constrained and different solutions are possible for the contribution of further resonances. Part of the problem results from a fairly large t-channel background contribution. Nevertheless, recently also the first measurement off the quasi-free neutron was reported from ELSA [110]. The total cross section and the coefficients of Legendre polynomials fitted to the angular distributions are compared to proton data and model results in Fig. 14. The results for proton and neutron are similar but indicate clearly different contributions in particular in the intermediate energy range. Also for the neutron final state, no unique solution could be obtained [110]. The measurement of polarization observables in the near future will help to solve this problem. The measurement of the quasi-free reaction off the neutron has shown that, in this channel, no significant nuclear effects will complicate such experiments. The quasi-free proton data are in excellent agreement with free proton data, even effects from Fermi motion are not significant at the current level of statistical precision [110].
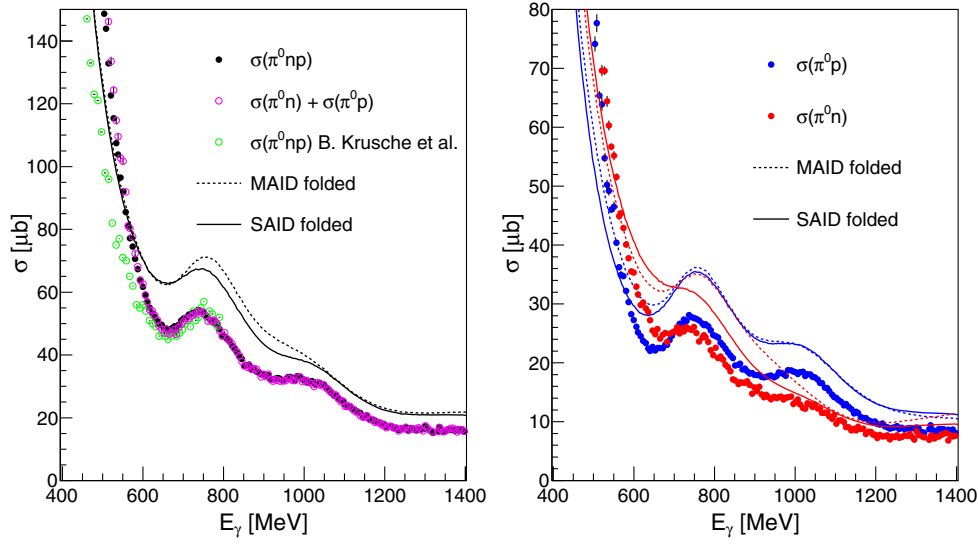
Fig. 15. Preliminary results for quasi-free photoproduction of π^0 mesons off the deuteron in the second and third resonance region [134]. Left hand side: inclusive $\gamma d \to np\pi^0$ data compared to sum of exclusive cross sections and results from MAID (dashed line) [41] and SAID (solid line) [35]. Both model results are for the incoherent sum of proton/neutron cross sections folded with Fermi motion. Right hand side: Same for exclusive quasi-free $\gamma p \to p\pi^0$ and $\gamma n \to n\pi^0$ reactions.

4.2 Meson photoproduction off the neutron – single π^0 production

The situation is completely different for the single π^0 channel, for which preliminary results [134] are shown in Fig. 15. We had already discussed in the introduction (sec. 1.1) that quasi-free inclusive data off the deuteron are not in agreement with the results from the MAID [41] or SAID [35] analyses, although the model results themselves are in fairly good agreement (as expected since they have been fitted to the same relatively large body of data available for the $\gamma p \to p\pi^0$, $\gamma p \to n\pi^+$, and $\gamma n \to p\pi^-$ reactions).

The left hand side of the figure demonstrates that the new preliminary quasi-free data for $\gamma p \to p\pi^0$ and $\gamma n \to n\pi^0$ sum up correctly to the inclusive cross section (the coherent part must still be separated, but is small at photon energies above 500 MeV) and that the inclusive data agree with the previous measurement (within systematic uncertainties). However, they clearly disagree with the MAID and SAID results (sum of proton and neutron cross section folded with Fermi motion). At the right hand side of the figure quasi-free proton and neutron cross sections are compared to the MAID and SAID results. For this reaction, throughout the second and third resonance region neither the proton nor the neutron data agree with the model results. Their energy dependence is similar, but on an absolute scale the data are lower than expected by roughly 25%. A similar result has been reported from the LNS experiment [135]. The model results agree very well with free proton data, to which they have been fitted. This means that quasi-free and free proton data disagree by ≈25% (and probably a similar effect occurs for the neutron). Interpretation of the quasi-free data thus will require detailed studies of nuclear effects on this reaction. Assuming that these effects are similar a comparison of the neutron/proton ratio from models and data might
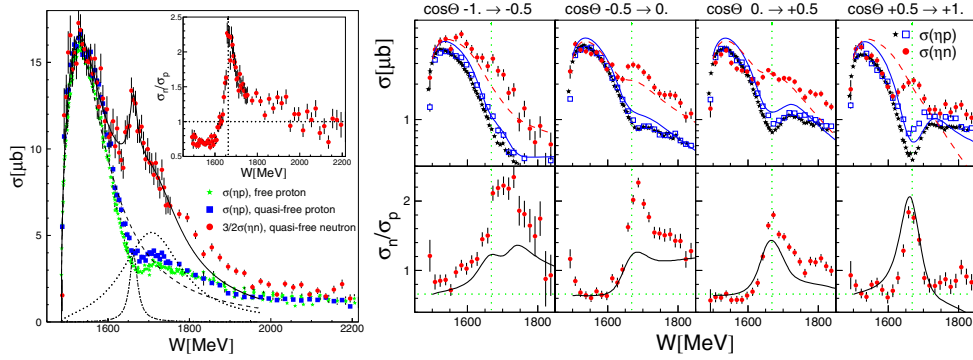
Fig. 16. Quasi-free photoproduction of η-mesons off the proton and neutron [127]. Left hand side: Total cross sections as function of final state invariant mass W (Red) dots: quasi-free neutron, (blue) squares: quasi-free proton, (green) stars: free proton data. Insert: ratio of quasi-free neutron–proton data. All curves for neutron data; dashed: fitted S_{11} line shape, dotted: broad Breit-Wigner resonance, dash-dotted: narrow Breit-Wigner, solid: sum of all. Right hand side: First row: excitation functions for different bins of η cm polar angle. (Blue) open squares: quasi-free proton data, (black) stars: free proton data from [147], (red) dots: quasi-free neutron data scaled up by 3/2. (Blue) solid lines: η-MAID [151] for the proton target, (red) dashed lines: η-MAID for the neutron target. Second row: ratio of neutron and proton cross section for data and η-MAID. Vertical dotted lines: position of narrow peak in neutron data, horizontal dotted lines: $\sigma_n/\sigma_p = 2/3$.

give results which are easier to interpret. The total cross sections already indicate different resonance contributions to the proton and neutron excitation.

4.3 Meson photoproduction off the neutron – the η-meson

Photoproduction of η mesons off the free proton has become a very well studied reaction over the last 15 years [14–17, 136–147]. It is particularly attractive due to the strong dominance of the $S_{11}(1535)$ resonance and (at least at moderate incident photon energies) comparably small contributions of non-resonant background terms. The main original motivation for the study of the $\gamma' n' \to' n'\eta$ reaction was related to the isospin structure of the $S_{11}(1535)$ resonance (see [30] for a summary) and model predictions [151] for a strong contribution of the $D_{15}(1675)$ resonance to the neutron excitations. However, when these experiments reached incident photon energies around 1 GeV an unexpected result was found. Measurements at GRAAL [148], Tohoku-LNS [130], ELSA [109, 127], and MAMI [149] revealed a prominent peak-like structure around $W \approx 1.7$ GeV, which has no counterpart for the proton.

The result for the total cross section from a new analysis of the ELSA data [127], using the kinematical reconstruction discussed above to eliminate the effects from Fermi motion, is shown at the right hand side of Fig. 16. A phenomenological fit of the data with the resonance shape of the $S_{11}(1535)$ resonance, a conventional Breit-Wigner that effectively subsumes the contributions from other broad resonances and non-resonant backgrounds, and an additional narrow Breit-Wigner curve results in a width (FWHM) of the narrow structure of only (25 ± 12) MeV; close to the experimental resolution. Also all other experiments have reported widths lower than ≈ 40 MeV.

The nature of this structure is not yet understood. Different scenarios involving contributions from specific resonances as well as interference patterns in the same

partial wave have been discussed in the literature. Fix, Tiator, and Polyakov [152] have investigated whether the data could be consistent with the excitation of a narrow P_{11}-state. This work was motivated by the idea that the P_{11}-state of the proposed anti-decuplet of pentaquark states should be relatively narrow (width of the order of 10 MeV), have a strong electromagnetic coupling to the neutron, and a large ηN decay branching ratio [153,154]. Due to Fermi smearing, they found solutions not only for narrow but also conventionally broad states. Similarly, an analysis performed in the framework of the Bonn-Gatchina model (BoGa) [155] can reproduce the data by either adding a 'conventionally' broad P_{11} resonance, a very narrow P_{11} state, or even by a careful adjustment of the interference pattern for the s-wave amplitudes. Shklyar, Lenske, and Mosel [156] found solutions just from coupled-channel effects in the S_{11}–P_{11} sector, without introducing any additional resonances. A similar result from a coupled-channel K-matrix approach was presented by Shyam and Scholten [157]. Finally, Döring and Nakayama [158], using an s-wave coupled channel model, find a 'dip-bump' structure in the neutron cross section related to the opening strangeness thresholds of $K\Lambda$ and $K\Sigma$ photoproduction around 900 MeV and 1050 MeV.

The scenarios with a contribution from one single conventionally broad resonance without intricate interference effects have been ruled out in the meantime by the data shown in Fig. 16. Also shown at the right hand side of Fig. 16 are excitation functions and neutron/proton ratios for four different ranges of the η cm polar angle. These data show that the structure is particularly strong for forward angles. A comparison to the most precise, recent free-proton data [147] reveals, that the peak-like structure for the neutron corresponds to a dip-like structure at the same W and with comparable width in the proton excitation functions. The similarity in the neutron-proton ratio between the data and the MAID prediction [151] results only from this proton dip, the neutron peak is not seen in the model results. This also causes some doubts, as to whether the proton dip is interpreted by the correct mechanism in the model.

In the meantime, an experiment at MAMI [150] has identified the same structure in quasi-free photoproduction off ^{3}He, i.e. in a different nuclear environment. This is shown in Fig. 17. The kinematic reconstruction of the neutron works less well for the helium target nucleus; one has to make the approximation that the pair of spectator nucleons in the four-body final state has no relative momentum. Due to this approximation, the resolution for the W excitation function is less good. However, the peak is still clearly visible and a more narrow width (close to the experimental resolution) can be recovered for the angular range where the neutron kinetic energy can be directly determined by the time-of-flight method (Fig. 17, lower right corner).

Finally, it should be mentioned that recently Kuznetsov and co-workers [159] have reported from the GRAAL experiment a similar structure in Compton scattering off the quasi-free neutron. If this structure is confirmed, it will impose significantly more stringent conditions on explanations with complicated interference patterns etc. which are not very likely to be identical for such different reaction channels.

Up to now, two important questions are open for this structure: what is its width on the free neutron and in which partial wave amplitude(s) does it appear. So far we have only upper limits for the widths. New data from MAMI [149] for quasi-free production off neutrons bound in the deuteron, which are still under analysis, have much better statistical quality than the previous experiments. This may help to further constrain the width by more detailed comparisons to the experimental resolution. The identification of the relevant amplitudes, and thus the quantum numbers of a prospective nucleon resonance, requires the measurement of polarization observables. This program has began in parallel in Mainz and Bonn, using deuterated frozen-spin butanol targets. First data have been taken in Bonn for the helicity dependence of
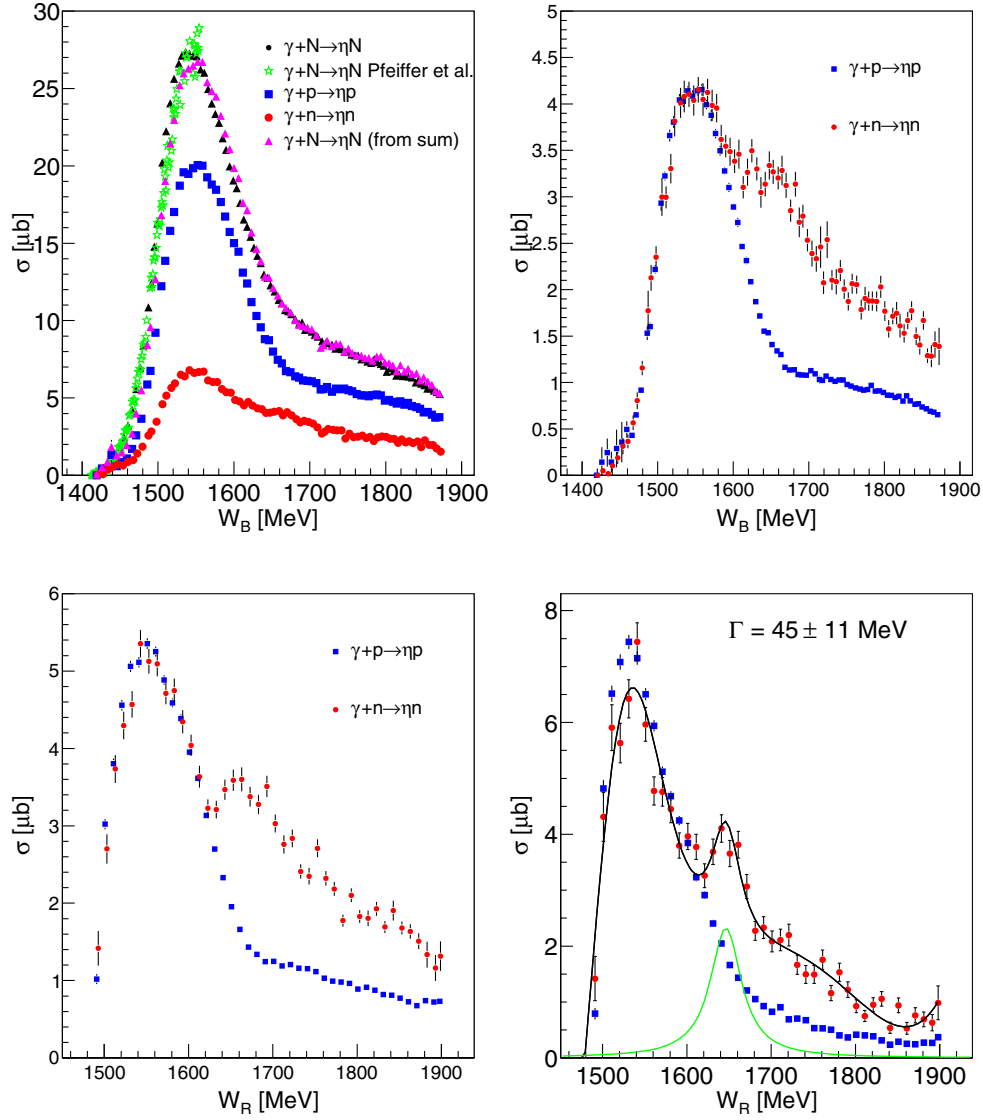
Fig. 17. Preliminary results for quasi-free η-photoproduction off ^{3}He [150]. Upper left: comparison of quasi-free cross sections off protons and neutrons with inclusive cross section. Previous data for inclusive reaction from Pfeiffer et al. [96]. Upper right: quasi-free proton and neutron cross sections (normalized in S_{11} peak) as function of W from E_γ (W_B). Lower left: same as function of W reconstructed from final state kinematics (W_R) (kinetic energy of neutron from reconstructed kinematics). Lower right: same as function of W_R for kinetic energy of neutron from time-of-flight measurement (only for η backward angles).

the cross section (observable E, circularly polarized beam on longitudinally polarized target), and in Mainz for the target asymmetry (transversely polarized target), and the double polarization observable F (transversely polarized target, circularly polarized beam).
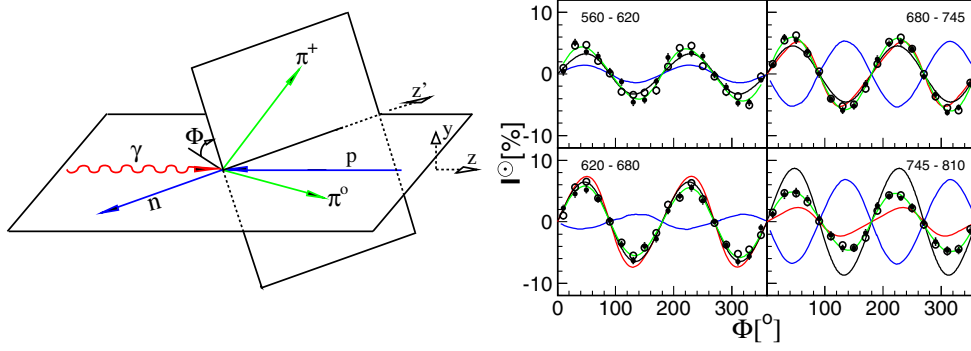
Fig. 18. Beam-helicity asymmetry for the double pion production off the nucleon [22]. Left hand side: definition of the angle Φ. Right hand side: results for the free proton compared to models. Curves: green: fit to data, black: Bonn-Gatchina model [19, 20], red: Fix and Arenhövel [173], blue: Roca [175].

4.4 Meson photoproduction off the neutron – double pion production

As already discussed in the introduction, photoproduction of pion pairs may allow the investigation of nucleon resonances which have only small branching ratios for decays to the nucleon ground state but decay dominantly to intermediate $N^\star$ or $\Delta^\star$ resonances. One expects that this scenario becomes more important the higher the excitation energy of the states. At the same time, for selected isospin channels, double pion production also gives access to ρ and σ meson decay channels. A large body of data has become available in particular for reactions off the free proton. For incident photon energies up to the second resonance region total cross sections and invariant-mass distributions of the $\pi\pi$- and the πN-pairs have been measured with the DAPHNE and TAPS detectors at the MAMI accelerator in Mainz [19, 160–166], and at higher incident photon energies at GRAAL in Grenoble (also the linearly polarized beam asymmetry) [18] and at ELSA in Bonn [19, 20]. Also the first double polarization observables (E, longitudinally polarized target, circularly polarized beam) have been measured in the context of the Gerasimov-Drell-Hearn project [167–169]. However, in spite of all these efforts even for the proton target in the low energy region the interpretation of the data is still strongly controversial. All models agree that the production of neutral pions involves smaller contributions from non-resonant terms like pion-pole diagrams or terms of the Δ-Kroll Rudermann type. But the reaction models do not even agree for the dominant contributions to the $\pi^0\pi^0$ channel. In the second resonance region, the model of the Valencia group [170–172] is dominated by the $D_{13}(1520) \to \Delta\pi^0 \to p\pi^0\pi^0$ reaction chain, Laget and co-workers [18] find a much more prominent contribution from the $P_{11}(1440) \to N\sigma$ decay, and the recent Bonn-Gatchina analysis [19] claims a large contribution from the $D_{33}(1700)$ state, which is almost negligible in the other models.

Several model predictions [172–175] indicated that polarization observables are extremely sensitive to the reaction mechanisms, but it came as a surprise when the first measurement of the beam helicity asymmetry of the $\gamma p \to p\pi^+\pi^-$ reaction at the CLAS facility [21] produced results that could not be reproduced by any reaction models. This observable can be measured for three-body final states with a circularly polarized photon beam on an unpolarized target and is defined by:

$$I^\odot(\Phi) = \frac{1}{P_\gamma}\frac{d\sigma^+ - d\sigma^-}{d\sigma^+ + d\sigma^-} = \frac{1}{P_\gamma}\frac{N^+ - N^-}{N^+ + N^-} \quad , \tag{9}$$
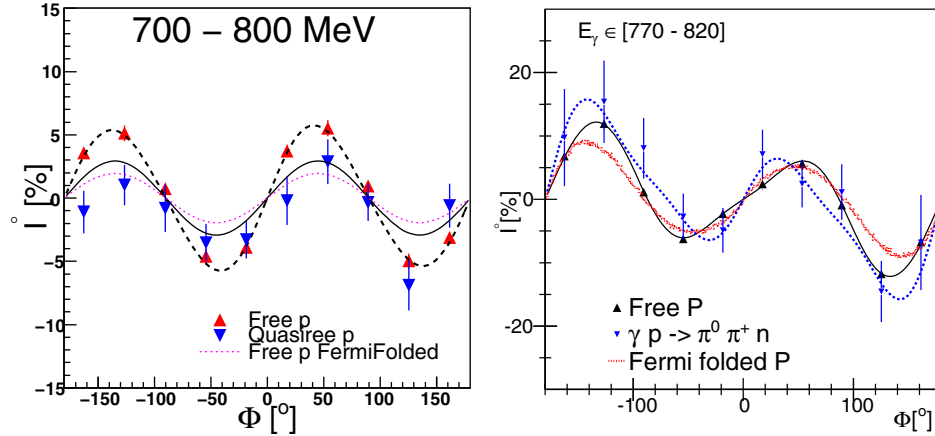
Fig. 19. Preliminary results for the beam-helicity asymmetry for quasi-free protons for the $p\pi^0\pi^0$ (left hand side) and the $n\pi^0\pi^+$ (right hand side) final states [179] compared to free proton results [22].

where $d\sigma^\pm$ is the differential cross section for each of the two photon helicity states, and P_γ is the degree of circular polarization of the photons. The definition of the angle Φ is shown in Fig. 18.

In the meantime [22] it has been found that, also for the $n\pi^0\pi^+$ final state all reaction models fail. For the $p\pi^0\pi^0$ final state at least some analyses (cf. Fig. 18) are close to the data, but also in this case the Valencia model [175], which is in good agreement with all other observables, is out of phase with the data.

The data base for reactions off the neutron is still much more sparse. At low incident photon energies total cross section data, invariant mass distributions, and the helicity dependence of the cross section for $\gamma n \to p\pi^-$ are available from Mainz [163,178]. Results for the $n\pi^0\pi^0$ final state have been reported from Mainz [176] and GRAAL [177].

New, precise results for total cross sections and invariant mass distributions for the quasi-free $\gamma n \to n\pi^0\pi^0$ reaction have been measured by the CBELSA experiment and are in preparation for publication [114]. Data for the same channel and for the $p\pi^-\pi^0$ final state have been also measured with the Crystal Ball/TAPS setup at MAMI up to photon energies of 1.4 GeV and are currently under analysis [179]. These data have been measured with circularly polarized photons, so that the above discussed beam-helicity asymmetry can be extracted. It was first shown that the results for this observable for quasi-free production off the bound deuteron also reproduce the free proton data. As demonstrated in Fig. 19 this is the case for both isospin channels. The final analysis of the quasi-free neutron data, using kinematical reconstruction to eliminate the Fermi motion effects, is under way. Initial, very preliminary results seem to indicate, that for the $\pi^0\pi^0$ channel the proton and neutron asymmetries are very similar, while they differ considerable for the mixed charged channel.

## 4.5 Coherent photoproduction off the deuteron $- \pi^0\eta$-pairs

Coherent photoproduction of mesons can give valuable additional information about the isospin structure of electromagnetic excitations, however, up to now, it has been little explored due to the, in general, very small cross sections. One such channel is the η photoproduction off light nuclei discussed in the next section in the context of η-mesic nuclei.
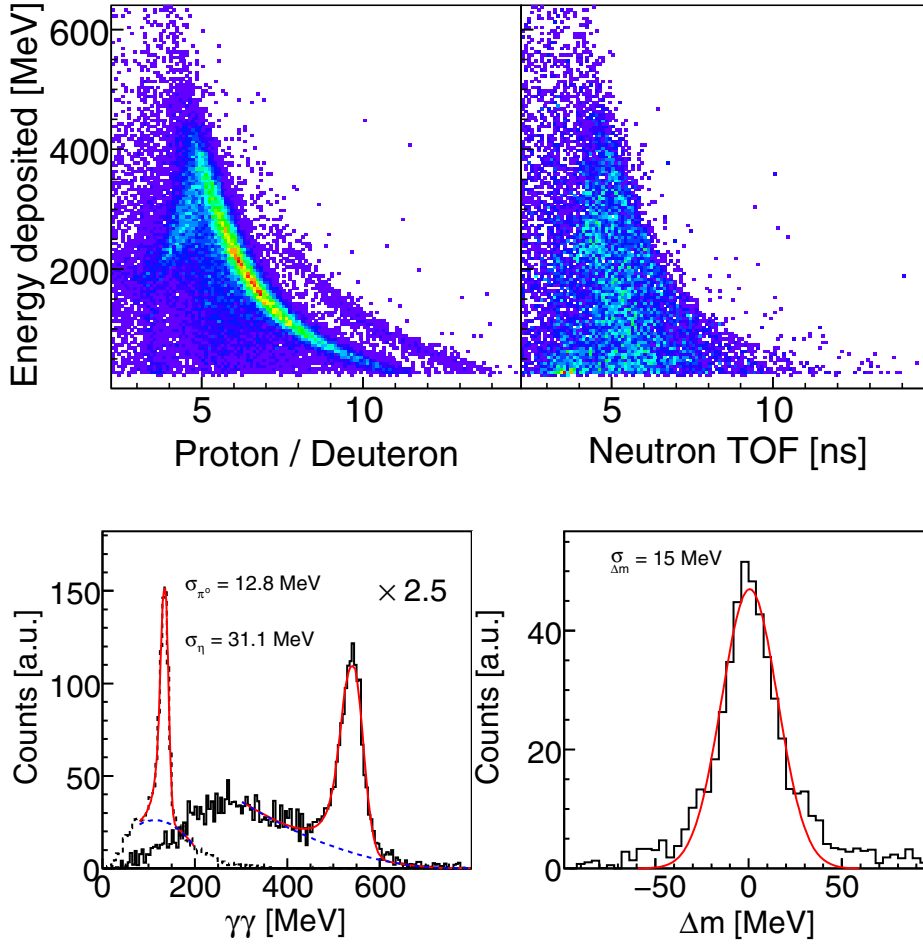
Fig. 20. Identification of the reaction $\gamma d \to d\pi^0\eta$ [115]. Upper part: time-of-flight versus energy for charged (left hand side) and neutral (right hand side) recoil particles. For the charged particles a prominent band for protons and a weaker band for neutrons is visible. Bottom part: left hand side: invariant mass spectra for π^0 and η mesons corresponding to the deuteron band in ToF-versus-E. Right hand side: missing mass spectrum after cut on invariant mass.

On the deuteron, this channel is suppressed by more than three orders of magnitude with respect to the elementary cross section off the free nucleon. One might therefore think, that the study of such a production process for multiple meson production reactions is hopeless. The contrary is the case, double π^0, $\eta\pi^0$, and even triple π^0 off the deuteron (and partly also off ^{3}He) have been identified recently. Here we will briefly discuss the $\gamma d \to d\eta\pi^0$ reaction.

Production of $\eta\pi^0$ pairs of the free proton was studied intensively during the last few years at GRAAL [23], ELSA [24,26,28], and MAMI [25,27]. Different model analyses of the data [24,27] found that the threshold region is strongly dominated by the decay of one single nucleon resonance, namely the $D_{33}(1700) \to P_{33}(1232)\eta \to N\eta\pi^0$ decay chain. The dominance is so strong that, so far, after the pion-decay of the Δ resonance and the η-decay of the $S_{11}(1535)$, this is the third case, where a resonance can be studied in great detail in one specific decay channel with low background contributions.
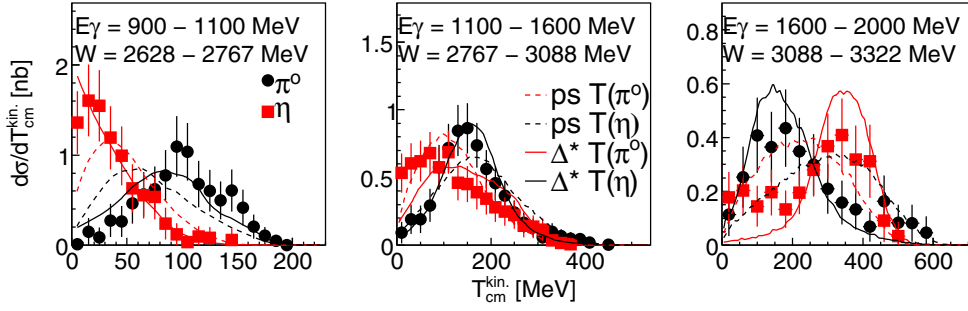
Fig. 21. Distribution of kinetic energies for π^0 (red squares) and η (black dots) mesons from $\gamma d \to d\pi^0\eta$ [115] for different bins of incident photon energy. The dashed curves are simulations assuming phase space, the solid curves assuming sequential decays of a $\Delta^\star$ via η emission to the $\Delta(1232)$.

The identification of the coherent reaction [115] in data from the CBELSA experiment is summarized in Fig. 20. The upper part of the figure shows energy-versus-time-of-flight spectra for recoil particles detected in TAPS in coincidence with $\pi^0\eta$ pairs. For charged recoil particles clear proton and deuteron bands are visible. The lower part of the figure shows at the left hand side the invariant mass signals for π^0 and η after a cut on the deuteron band and at the right hand side the missing mass spectrum after cuts on the pion and eta invariant masses. This spectrum is not only almost background free, the narrow width of the peak also proves that only the coherent reaction has been selected (the quasi-free reaction has broader peaks due to Fermi smearing).

In view of resonance excitations, the coherent reaction adds additional isospin selectivity. The final $d\eta\pi^0$ state has isospin $I = 1$. This means that the resonance excitation must have been isospin changing from the $I = 0$ deuteron to an $I = 1$ $d^\star$, which is only possible for the excitation of a Δ resonance. Thus processes like $\gamma N \to N^\star \to S_{11}(1535)\pi \to N\eta\pi^0$, which contribute to the elementary reaction are isospin forbidden.

Kinetic energy spectra of the pions and η mesons from the coherent reaction are shown in Fig. 21. They support the sequential decay scenario of the $D_{33}(1700)$ resonance. The kinetic energies of the pions always peak at energies corresponding to the decay of the Δ resonance, while the kinetic energies of the η mesons shift upwards with increasing incident photon energies, scanning the line shape of the $D_{33}(1700)$ resonance.

4.6 Meson photoproduction off nuclei

4.6.1 η-mesic nuclei

We have discussed in the introduction in detail the search for η-nucleus (quasi-)bound states, so-called η-mesic nuclei. Tentative evidence, although at low statistical quality, for such states had been reported from a measurement of meson photoproduction off ^{3}He by Pfeiffer and co-workers [96] with the TAPS detector at MAMI. This experiment has been repeated with much higher statistical quality and a larger incident photon energy coverage with the Crystal Ball/TAPS experiment at MAMI [180]. The most important experimental findings are summarized in Fig. 22.
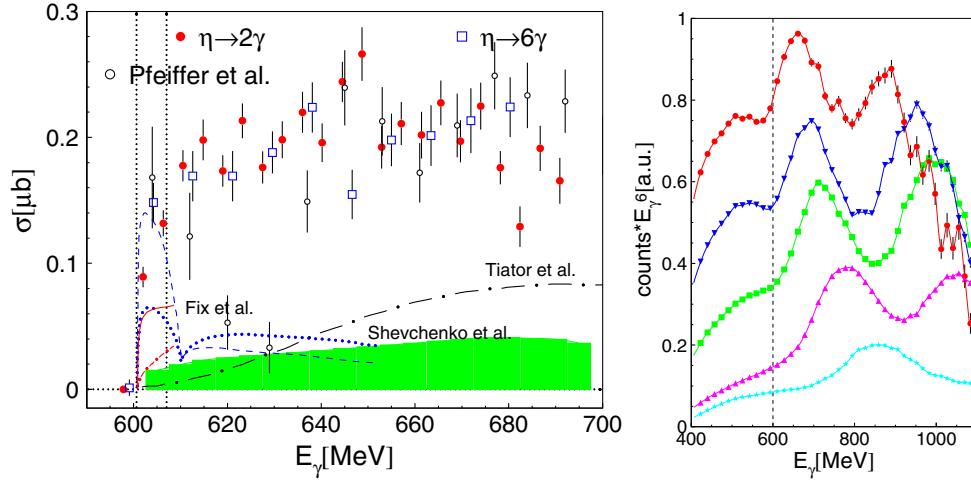
Fig. 22. Left hand side: preliminary total cross section for the $\gamma^3\text{He} \rightarrow^3 \text{He}\eta$ reaction from $\eta \rightarrow 2\gamma$ and $\eta \rightarrow 6\gamma$ decays [180]. The shaded band at the bottom indicates the systematic uncertainty. The two vertical lines indicate coherent and breakup threshold. Previous data from Pfeiffer et al. [96]. Theory curves: (blue) dotted and dashed from Shevchenko et al. [181] for two different versions of elastic ηN scattering, (red) solid (dash-dotted): Fix and Arenhövel [182] full model (plane wave), (black) long dash-dotted: Tiator et al. [183]. Right hand side: excitation functions of $\pi^0 - p$ back-to-back pairs for different ranges of the opening angle $\Psi_{\pi p}$ after removal of the overall energy dependence $\propto E_\gamma^{-6}$. From top to bottom opening angle ranges of: $165°$–$180°$, $150°$–$165°$, $140°$–$150°$, $130°$–$140°$, and $120°$–$130°$. Vertical lines: η-production threshold.

The left hand side of the figure shows the total cross section for the coherent $\gamma^3\text{He} \rightarrow \eta^3\text{He}$ reaction extracted from the two-photon and three-pion decays of the η-meson. Both data sets are in good agreement and confirm the extremely sharp rise of the excitation function at the kinematic threshold for coherent η production. The data are also in reasonable agreement with the previous experiment by Pfeiffer et al. [96], although they do not show the dip-like structure in the previous data at incident photon energies around 620 MeV. Here, one should note that, in this range, the systematic uncertainty in the previous data was comparably large because the coherent signal had to be extracted by fitting a small coherent contribution in the missing energy spectra, which were dominated by the quasi-free reaction. At lower incident photon energies, the quasi-free contribution is relatively much smaller and at higher incident energies it is better separated from the coherent component. The present experiment profited not only from the better statistics but also from the almost 4π coverage of the detector system, which allowed the removal of a significant fraction of the quasi-free background by the detection of associated recoil nucleons. Altogether, the extraordinary threshold behavior of this reaction, which is very similar to the hadron induced reactions [90–92], was confirmed and supports the assumption of a resonant behavior at threshold. In the figure, the data are also compared to the results of different models. The plane-wave models (Tiator and co-workers [183], Fix and Arenhövel [182]) have a completely different energy dependence in the threshold region. The model of Fix and Arenhövel, including final state interactions, reproduces a very steep slope at threshold, but does not agree with the magnitude of the cross section in that region. Also the models by Shevchenko et al. [181] for two different versions of elastic ηN re-scattering show a steep rise at threshold; but can reproduce neither energy dependence nor magnitude of the data over a larger energy range. The differential cross section data (not shown), confirm also the previous finding.

The angular dependence at higher incident photon energies is dominated by forward peaking related to the nuclear form factor. But in the threshold region they are much more isotropic and very close to threshold they show a behavior which is opposite to what is expected from the form factor. This is evidence for at least strong FSI effects in the threshold region.

The other tentative signature for the formation of a quasi-bound state reported by Pfeiffer et al. [96] was a small, narrow peak-like structure at the coherent η production threshold in the excitation function of proton-π^0 pairs emitted back-to-back in the photon-^{3}He cm system. The interpretation of this structure is related to the following picture. When a quasi-bound η-nucleus state forms, the η may be re-captured by a nucleon which is then excited to the $S_{11}(1535)$ resonance with a large probability. This resonance has very similar decay branching ratios into $N\pi$ and $N\eta$ (both in the range between 45% and 55% [184]). That means the S_{11} can either re-emit the η or a pion. Due to the small mass of the pion, its emission is also possible below the coherent η production threshold, where the decay into $N\eta$ necessarily leads again to the formation of a bound system. Therefore, while in coherent η production we observe only the abrupt rise of the cross section at threshold, in the pion channel a peak may occur, which is indicative for the width of the resonant structure. There is, however, even after appropriate kinematical cuts, a large background from quasi-free single π^0 production. In the work of Pfeiffer et al. a large part of this background was subtracted with a side-band analysis: the excitation function for $\pi^0 - p$ pairs with opening angles between 150°–170° was subtracted from the one between 170°–180° after proper normalization. The idea was, that the background from quasi-free π^0 production changes only slowly with the opening angles. An analysis of the same type applied to the new high statistics data reproduces the peak observed in [96] with much higher statistical significance. However, the new data allow also a more detailed study of the quasi-free single π^0 background. This is shown in Fig. 22, right hand side. The excitation functions for different pion - proton opening angle Ψ have been constructed after cuts on the reaction kinematics, which enhance the possible signal from η-mesic nuclei with respect to the quasi-free background. The overall energy dependence in the range of interest on the order of E_γ^{-6} has been removed. The figure shows clearly remnant structures from the bumps of the second and third resonance region in quasi-free pion production. These structures move unfortunately with decreasing opening angle to higher incident photon energies. This is a trivial kinematic effect because changing opening angles require different combinations of incident photon energy and nuclear Fermi momentum to produce the same value of W. Since the nucleon resonance bumps are at fixed positions in W, they must shift with E_γ as function of Ψ. The peak reported by Pfeiffer et al. [96] occurs exactly at the coherent η production threshold. But the back-to-back pairs (165°–180°) do not show a peak at this position, rather the rising slope of the low energy tail of the second resonance region. At the same position the 150°–165° data are not yet in this rising slope but by chance in a little dip just before it. Subtraction of the scaled background thus produces a narrow peak-like structure at threshold, which is however artificially caused by the dip in the background. A true signal from an η-mesic state would be somewhere hidden in these complicated structures, and there is almost no hope to extract such a signal.

A final remark should be made to the search for η-mesic states in other light nuclei. The use of photon induced η-production restricts possible target nuclei to spin $J \neq 0$ and isospin $I \neq 0$ nuclei like ^{3}He because the dominant amplitude is an isovector spin-flip. The next best candidate would be ^{7}Li. Such data from the Crystal Ball/TAPS experiment at MAMI are in preparation for publication [185]. Also in this case a significant enhancement of the cross section in the threshold region was observed, although not as dramatic as for the ^{3}He nucleus.

It would be even more interesting, to search for η-mesic states in the much more strongly bound ^{4}He. However, as discussed above, in this case coherent η-production is not a possible entrance channel. Nevertheless, in this case the coherent production of $\pi^0\eta$ pairs discussed in the previous section could possibly be explored. Since this reaction is dominated near threshold by the process $\gamma N \to D_{33}(1700) \to P_{33}(1232)\eta \to N\eta\pi^0$ the electromagnetic excitation must go via the $V3$ amplitude, which is identical for protons and neutrons so that no cancellation can occur. Since D_{33} and P_{33} have opposite parity but the same total angular momentum, the $D_{33} \to \eta P_{33}$ transition is s-wave ($J = 0$ η meson with negative intrinsic parity). The subsequent $P_{33} \to N$ transition is the usual magnetic p-wave decay of the Δ resonance known from single pion production. Consequently, coherent production of $\eta\pi^0$ pairs is not suppressed for the scalar isoscalar ^{4}He nucleus. An additional advantage of this reaction is, that one can select events, where the pion carries away most of the momentum, so that the η-meson has only a small momentum relative to the nucleus, as needed for the formation of a quasi-bound state.

4.6.2 Photoproduction of pion pairs off nuclei

New, precise data have been obtained with Crystal Ball/TAPS at MAMI for the photoproduction of neutral and mixed charged pion pairs of a series of nuclei (^{2}H, ^{7}Li, ^{12}C, ^{40}Ca, ^{93}Nb, and ^{nat}Pb. The main purpose of this experiment was to collect further data which give some clues to distinguish between trivial FSI effects and genuine in-medium modifications of the σ meson in the pion-pion invariant mass distributions. Compared to the results by Messchendorp et al. [57] and Bloch and coworkers [58] the present data [185] improve the situation in two aspects. The much better statistical quality does not only provide more significant signals in the invariant mass distributions but also allows the study of these effects more systematically to low incident photon energies. The addition of the light nuclei (^{2}H, ^{7}Li) gives better reference points for low average nuclear density, where in-medium effects of the σ should not play an important role.

Preliminary results for the invariant mass distributions are compared in Fig. 23 for the $\pi^0\pi^0$ and the $\pi^0\pi^\pm$ final states for four different ranges of incident photon energies from the immediate threshold region at 300 MeV up to 500 MeV. They can be summarized in the following way. For both isospin channels the invariant mass distributions of different target nuclei are very similar; there is not even much difference between the deuteron (basically proton/neutron average of elementary cross sections) and lead nuclei. At these very low incident photon energies, the produced pions must have small momenta, below the threshold where they could excite the Δ-resonance. This means, that as discussed in the introduction (cf Fig. 8), they are almost unaffected by FSI effects. Nevertheless, possible in-medium effects of the σ meson should also occur in this region. Towards higher photon energies, the picture changes completely. In particular the $\pi^0\pi^0$ invariant mass distributions for heavy nuclei develop a very significant low mass enhancement with respect to the light nuclei. This effect is also visible for the mixed charge channel, although less pronounced. This picture is consistent with the FSI effects, in particular from quasi-elastic charge-exchange scattering of the pions, discussed in the introduction. They increase with incident photon energy, are more important for $\pi^0\pi^0$ than for $\pi^0\pi^\pm$ (because of the relative size of the cross sections of feeding and fed channels), and give rise to enhancements at low invariant masses. Although a detailed comparison to models must still be done, the preliminary results seem to indicate that the observed effects are mainly related to pion-FSI.
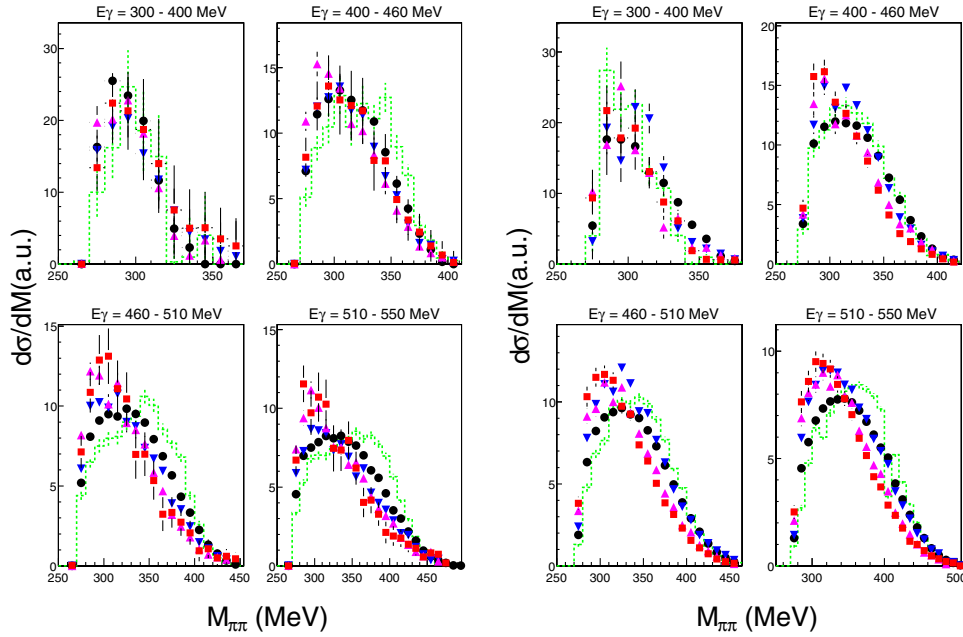
Fig. 23. Preliminary invariant mass distributions of $\pi^0\pi^0$ pairs (left hand side) and $\pi^0\pi^+$ pairs (right hand side) off nuclei for different ranges of incident photon energy (all distributions normalized to total cross section [185]. (Green) histograms: deuterium, (black) dots: ^{7}Li, (blue) downward triangles: ^{12}C, (magenta) upward triangles: ^{40}Ca, (red) squares: ^{nat}Pb.

5 Conclusions and outlook

We have discussed in this paper the two main aspects of a world-wide active program for the study of photon induced meson production reactions off nuclear targets: the study of the electromagnetic excitations of the neutron and the investigation of meson-nucleus interactions and meson in-medium properties. Many new results have become available during the last few years and much more is to come in the near future.

The measurement of meson production reactions off quasi-free nucleons has been put on a much more systematic basis, in particular by the detailed study of nuclear effects on the quasi-free proton cross sections which can be compared to their free counter parts. Effects from nuclear Fermi motion can be reliably removed by kinematic reconstruction techniques. The picture for nuclear effects beyond Fermi motion is not unique. For some reactions like η- and η'-production they do not seem to play any role. For other reactions, as in example single π^0 photoproduction, they seem to be substantial, so that in this case it is probably better to compare the less affected neutron/proton ratios to model predictions. Already measured data from the CBELSA (Bonn) and Crystal Ball (Mainz) experiments for many further final states ($n\pi^0$, $n\omega$, $n\pi^0\pi^0$, $p\pi^0\pi^-$, $n\pi^0\eta$, $p\pi^-\eta$) from photoproduction off the neutron are currently under analysis and will soon become available. Furthermore, currently, at both experiments, first beam times with a polarized deuterated butanol target for the measurements of (double) polarization experiments are under way and will continue in 2011/2012. These data will greatly extend the data base for photoproduction reactions on the neutron and should help to solve urgent questions like the nature of the narrow structure in the excitation function of η-photoproduction off the neutron.

New data for the measurement of coherent photoproduction off light nuclei serving as isospin filters will also become available soon. These reaction channels have recently

been investigated for the first time for the production of meson pairs and triples like $\pi^0\pi^0$, $\pi^0\eta$, and $\pi^0\pi^0\pi^0$.

The measurement of meson-nucleus interactions is also continuing. New results for the interaction of η' mesons in nuclei will be published soon. The question of the existence of η-mesic nuclei is not yet finally solved. The new precise results for coherent η photoproduction off ^{3}He nuclei have confirmed the extraordinary threshold behavior of this reaction, but the existence of a related structure in the excitation function of π^0-proton back-to-back pairs could not be confirmed. New results for ^{7}Li will become available soon, and experiments are planned to search for η-mesic ^{4}He using the $\pi^0\eta$ production reaction. Furthermore, data are under analysis to study for the first time the threshold behavior of η' production off the deuteron and off ^{3}He. Finally, detailed investigations of the production of pion pairs off light and heavy nuclei, although not yet complete, seem to indicate that the previously observed effects in the invariant mass spectra of the meson pairs are due to final state interaction effects, rather than to in-medium modifications of the σ meson.

References

1. S. Leupold, V. Metag, U. Mosel, Int. J. Mod. Phys. E **19**, 147 (2010)
2. B. Krusche, Prog. Part. Nucl. Phys. **55**, 46 (2005)
3. D. Drechsel, et al., Nucl. Phys. A **660**, 423 (1999)
4. B. Krusche, et al., Phys. Lett. B **526**, 287 (2002)
5. B. Krusche, Eur. Phys. J A **26**, 7 (2005)
6. C.M. Tarbert, et al., Phys. Rev. Lett. **100**, 0132301 (2008)
7. S. Dürr, et al., Science **322**, 1224 (2008)
8. T. Burch, et al., Phys. Rev. D **74**, 014504 (2006)
9. S. Basak, et al., Phys. Rev. D **76**, 074504 (2007)
10. J. Bulava, et al., Phys. Rev. D **82**, 014507 (2010)
11. S. Capstick, W. Roberts, Prog. Part. Nucl. Phys. **241**, 241 (2000)
12. E. Klempt, J.M. Richard, Rev. Mod. Phys. **82**, 1095 (2010)
13. B. Krusche, et al., Phys. Lett. B **397**, 171 (1997)
14. B. Krusche, et al., Phys. Rev. Lett. **74**, 3736 (1995)
15. M. Dugger, et al., Phys. Rev. Lett. **89**, 222002 (2002)
16. M. Williams, et al., Phys. Rev. C **80**, 045213 (2009)
17. V. Crede, et al., Phys. Rev. C **80**, 055202 (2009)
18. Y. Assafiri, et al., Phys. Rev. Lett. **90**, 222001 (2003)
19. A.V. Sarantsev, et al., Phys. Lett. B **659**, 94 (2008)
20. U. Thoma, et al., Phys. Lett. B **659**, 87 (2008)
21. S. Strauch, et al., Phys. Rev. Lett. **95**, 162003 (2005)
22. D. Krambrich, et al., Phys. Rev. Lett. **103**, 052002 (2009)
23. J. Ajaka, et al., Phys. Rev. Lett. **100**, 052003 (2008)
24. I. Horn, et al., Eur. Phys. J. A **38**, 173 (2008)
25. V.L. Kashevarov, et al., Eur. Phys. J. A **42**, 141 (2009)
26. E. Gutz, et al., Phys. Lett. B **687**, 11 (2010)
27. V.L. Kashevarov, et al., Phys. Lett. B **693**, 551 (2010)
28. I. Horn, et al., Phys. Rev. Lett. **101**, 202002 (2008)
29. K.M. Watson Phys. Rev. **85**, 852 (1952)

30. B. Krusche, S. Schadmand Prog. Part. Nucl. Phys. **51**, 399 (2003)
31. R.G. Moorehouse, Phys. Rev. Lett. **16**, 772 (1966)
32. N. Bianchi, et al., Phys. Rev. C **54**, 1688 (1996)
33. T.A. Armstrong, et al., Phys. Rev. D **5**, 1640 (1972)
34. M. MacCormick, et al., Phys. Rev. C **53**, 41 (1996)
35. R.A. Arndt, et al., Phys. Rev. C **66**, 055213 (2002) SAID homepage:
    `http://gwdac.phys.gwu.edu/`
36. P. Benz, et al., Nucl. Phys. B **65** (1997) 158
37. W. Chen, et al., Phys. Rev. Lett. **103**, 012301 (2009)
38. M. Fuchs, et al., Phys. Lett. B **386**, 20 (1996)
39. B. Krusche, et al., Eur. Phys. J. A **6**, 309 (1999)
40. K. Büchler, et al., Nucl. Phys. A **570**, 580 (1994)
41. D. Drechsel, et al., Nucl. Phys. A **645**, 145 (1999)
42. E.M. Darwish, H. Arenhövel, M. Schwamb, Eur. Phys. J. A **16**, 111 (2003)
43. V.E. Tarasov, et al. [`arXiv:1105.0225`] (2011)
44. B. Krusche, et al., Eur. Phys. J. A **22**, 277 (2004)
45. M. Röbig-Landau, et al., Phys. Lett. B **373**, 45 (1996)
46. T. Mertens, et al., Eur. Phys. J. A **38**, 195 (2008)
47. M. Kotulla, et al., Phys. Rev. Lett. **100**, 192302 (2008)
48. T. Ishikawa, et al., Phys. Lett. B **608**, 215 (2005)
49. O. Buss, et al., Eur. Phys. J. A **29**, 189 (2006)
50. V. Bernard, U.-G. Meissner, I. Zahed, Phys. Rev. Lett. **59**, 966 (1987)
51. F. Bonutti, et al., Phys. Rev. Lett. **77**, 603 (1996)
52. F. Bonutti, et al., Phys. Rev. C **60**, 018201 (1999)
53. F. Bonutti, et al., Nucl. Phys. A **677**, 213 (2000)
54. P. Camerini, et al., Nucl Phys A **735**, 89 (2004)
55. N. Grion, et al., Nucl. Phys. A **763**, 80 (2005)
56. A. Starostin, et al., Phys. Rev. Lett. **85**, 5539 (2000)
57. J.G. Messchendorp, et al., Phys. Rev. Lett. **89**, 222302 (2002)
58. F. Bloch, et al., Eur. Phys. J. A **32**, 219 (2007)
59. H. Geissel, et al., Phys. Rev. Lett. **88**, 122301 (2002)
60. E. Marco, W. Weise., Phys. Lett. B **502**, 59 (2001)
61. R.S.Bhalerao, L.C. Liu, Phys. Rev. Lett. **54**, 865 (1985)
62. L.C. Liu, Q. Haider, Phys. Rev. C **34**, 1845 (1986)
63. R.E.Chrien, et al., Phys. Lett. B **60**, 2595 (1988)
64. J.D.Johnson, et al., Phys. Rev. C **47**, 2571 (1993)
65. G.A. Sokol, et al., Fizika B **8**, 85 (1999)
66. G.A. Sokol, L.N. Palyuchenko, Phys. Atom. Nucl. **71**, 509 (2008)
67. B. Krusche, et al., Phys. Lett. B **358**, 40 (1995)
68. P. Hoffmann-Rothe, et al., Phys. Rev. Lett. **78**, 4697 (1997)
69. J. Weiss, et al., Eur. Phys. J. A **11**, 371 (2001)
70. J. Weiss, et al., Eur. Phys. J. A **16**, 275 (2003)
71. V. Hejny, et al., Eur. Phys. J. A **6**, 83 (1999)
72. V. Hejny, et al., Eur. Phys. J. A **13**, 493 (2002)
73. R.A. Arndt, et al., Phys. Rev. C **72**, 045202 (2005)
74. T. Ueda, Phys. Rev. Lett. **66**, 297 (1991)
75. T. Ueda, Phys. Lett. B **291**, 228 (1992)
76. C. Wilkin, Phys. Rev. C **47**, R938 (1993)
77. S.A. Rakityanski, et al., Phys. Lett. B **359**, 33 (1995)
78. S.A. Rakityanski, et al., Phys. Rev. C **53**, R2043 (1996)
79. A.M. Green, S. Wycech, Phys. Rev. C **54**, 1970 (1996)
80. N.N. Scoccola, D.O. Riska, Phys. Lett. B **444**, 21 (1998)
81. N.V. Shevchenko, et al., Eur. Phys. J. A **9**, 143 (2000)
82. V.Yu. Grishina, et al., Phys. Lett. B **475**, 9 (2000)
83. H. Garcilazo, M.T. Pena, Phys. Rev. C **63**, 021001(R) (2001)

84. H. Calén, et al., Phys. Lett. B **366**, 366 (1996)
85. J. Smyrski, et al., Phys. Lett. B **474**, 182 (2000)
86. P. Moskal, et al., Phys. Rev. C **69**, 025203 (2004)
87. F. Plouin, et al., Phys. Rev. Lett. **65**, 690 (1990)
88. H. Calén, et al., Phys. Rev. Lett. **80**, 2069 (1998)
89. B. Mayer, et al., Phys. Rev. C **53**, 2068 (1996)
90. J. Smyrski, et al., Phys. Lett. B **649**, 258 (2007)
91. T. Mersmann, et al., Phys. Rev. Lett. **98**, 242301 (2007)
92. T. Rausmann, et al., Phys. Rev. C **80**, 017001 (2009)
93. N. Willis, et al., Phys. Lett. B **406**, 14 (1997)
94. C. Wilkin, et al., Phys. Lett. B **654**, 92 (2007)
95. F. Hibou, et al., Eur. Phys. J. A **7**, 537 (2000)
96. M. Pfeiffer, et al., Phys. Rev. Lett. **92**, 252001 (2004)
97. H. Herminghaus, et al., IEEE Trans. Nucl. Sci. **30**, 3274 (1983)
98. K.-H. Kaiser, et al., Nucl. Inst. Meth. A **593**, 159 (2008)
99. I. Anthony, et al., Nucl. Inst. Meth. A **301**, 230 (1991)
100. A. Starostin, et al., Phys. Rev. C **64**, 055205 (2001)
101. R. Novotny, IEEE Trans. Nucl. Sci. **38**, 379 (1991)
102. A.R. Gabler, et al., Nucl. Instr. Meth. A **346**, 168 (1994)
103. D. Watts, in *Calorimetry in Particle Physics, Proceedings of the 11th Internatinal Conference, Perugia, Italy 2004*, edited by C. Cecchi, P. Cenci, P. Lubrano, M. Pepe (World Scientific, Singapore, 2005), p. 560
104. D. Husman, W.J. Schwille, Phys. BL. **44**, 40 (1988)
105. W. Hillert, Eur. Phys. J. A **28**, 139 (2006)
106. D. Elsner, et al., Eur. Phys. J. A **39**, 373 (2009)
107. E. Aker, et al., Nucl. Instr. Meth. A **321**, 69 (1992)
108. G. Suft, et al., Nucl. Inst. Meth. A **538**, 416 (2005)
109. I. Jaegle, et al., Phys. Rev. Lett. **100**, 252002 (2008)
110. I. Jaegle, et al., Eur. Phys. J. A **47**, 11 (2011)
111. D. Trnka, et al., Phys. Rev. Lett. **94**, 192303 (2005)
112. M. Nanova, et al., Phys. Rev. C **82**, 035209 (2010)
113. M. Nanova, et al., Eur. Phys. Lett. **47**, 16 (2011)
114. I. Jaegle, et al. (in preparation)
115. I. Jaegle, Cin. Phys. C **33**, 1340 (2009)
116. B.A. Mecking, et al., Nucl. Inst. Meth. A **503**, 513 (2003)
117. R. Nasseripour, et al., Phys. Rev. Lett. **99**, 262302 (2007)
118. M.H. Wood, et al., Phys. Rev. C **78** (2008) 015201
119. F. Hinode, et al., edited by W.B. Liu et al., Proceedings of the Second Asian Particle Accelerator Conf. (2001), p. 106
120. H. Yamazaki, et al., Nucl. Inst. Meth. A **536**, 70 (2005)
121. T. Kinoshita, et al., Phys. Lett. B **639**, 429 (2006)
122. K. Suzuki, et al., Mod. Phys. Lett. A **24**, 978 (2009)
123. M. Sumihama, et al., Phys. Rev. C **73**, 035214 (2006)
124. T. Nakano, et al., Phys. Rev. Lett. **91**, 012002 (2003)
125. O. Bartalini, et al., Eur. Phys. J. A **26**, 399 (2005)
126. A. Fantini, et al., Phys. Rev. C **78**, 015203 (2008)
127. I. Jaegle, et al., Eur. Phys. J. A (accepted)
128. C. Zeitnitz, et al., The GEANT-CALOR interface user's guide (2001) (`http://www.staff.uni-mainz.de/zeitnitz/Gcalor/gcalor.html`)
129. F. Wissmann, et al., Nucl. Phys. A **660**, 232 (1999)
130. F. Miyahara, et al., Prog. Theor. Phys. Suppl. **168**, 90 (2007)
131. K. Nakayama, H. Haberzettl, Phys. Rev. C **73**, 045211 (2006)
132. W.T. Chiang, et al., Phys. Rev. C **68**, 045202 (2003)
133. M. Dugger, et al., Phys. Rev. Lett. **96**, 169905 (2006)
134. M. Dieterle, Master Thesis, Univ. Basel (2010) (to be published)

135. H. Shimizu, talk presented at Narrow Nucleon Resonance Workshop, Edinburgh (2009)
136. J. Ajaka, et al., Phys. Rev. Lett. **81**, 1797 (1998)
137. A. Bock, et al., Phys. Rev. Lett. **81**, 534 (1998)
138. C.S. Armstrong, et al., Phys. Rev. D **60**, 052004 (1999)
139. R. Thompson, et al., Phys. Rev. Lett. **86**, 1702 (2001)
140. F. Renard, et al., Phys. Lett. B **528**, 215 (2002)
141. V. Crede, et al., Phys. Rev. Lett. **94**, 012004 (2005)
142. T. Nakabayashi, et al., Phys. Rev. C **74**, 035202 (2006)
143. O. Bartholomy, et al., Eur. Phys. J. A **33**, 133 (2007)
144. D. Elsner, et al., Eur. Phys. J. A **33**, 147 (2007)
145. H. Denizli, et al., Phys. Rev. C **76**, 015204 (2007)
146. M. Sumihama, et al., Phys. Rev. C **80**, 052201(R) (2009)
147. E.F. McNicoll, et al., Phys. Rev. C **82**, 035208 (2010)
148. V. Kuznetsov, et al., Phys. Lett. B **647**, 23 (2007)
149. D. Werthmüller, Cin. Phys. C **33**, 1345 (2009)
150. L. Witthauer, Master Thesis, Univ. Basel (2010) (to be published)
151. W.-T. Chiang, et al., Nucl. Phys. A **700**, 429 (2002)
152. A. Fix, L. Tiator, M.V. Polyakov, Eur. Phys. J. A **32**, 311 (2007)
153. M. Polyakov, A. Rathke, Eur. Phys. J. A **18**, 691 (2003)
154. R.A. Arndt, et al., Phys Rev C **69**, 035208 (2004)
155. V.A. Anisovich, et al., Eur. Phys. J. A **41**, 13 (2009)
156. V. Shklyar, H. Lenske, U. Mosel, Phys. Lett. B **650**, 172 (2007)
157. R. Shyam, O. Scholten, Phys. Rev. C **78**, 065201 (2008)
158. M. Döring, K. Nakayama, Phys. Lett. B **683**, 145 (2010)
159. V. Kuznetsov, et al., Phys. Rev. C **83**, 022201(R) (2011)
160. A. Braghieri, et al., Phys. Lett. B **363**, 46 (1995)
161. F. Härter, et al., Phys. Lett. B **401**, 229 (1997)
162. A. Zabrodin, et al., Phys. Rev. C **55**, R1617 (1997)
163. A. Zabrodin, et al., Phys. Rev. C **60**, 055201 (1999)
164. M. Wolf, et al., Eur. Phys. J. A **9**, 5 (2000)
165. W. Langgärtner, et al., Phys. Rev. Lett. **87**, 052001 (2001)
166. M. Kotulla, et al., Phys. Lett. B **578**, 63 (2004)
167. J. Ahrens, et al., Phys. Lett. B **551**, 49 (2003)
168. J. Ahrens, et al., Phys. Lett. B **624**, 173 (2005)
169. J. Ahrens, et al., Eur. Phys. J. A **34**, 11 (2007)
170. J.A. Gomez Tejedor, E. Oset, Nucl. Phys. A **600**, 413 (1996)
171. J.C. Nacher, et al., Nucl. Phys. A **695**, 295 (2001)
172. J.C. Nacher, E. Oset, Nucl. Phys. A **697**, 372 (2002)
173. A. Fix, H. Ahrenhövel, Eur. Phys. J. A **25**, 115 (2005)
174. W. Roberts, T. Oed, Phys. Rev. C **71**, 055201 (2005)
175. L. Roca, Nucl. Phys. A **748**, 192 (2005)
176. V. Kleber, et al., Eur. Phys. J. A **9**, 1 (2000)
177. J. Ajaka, et al., Phys. Lett. B **651**, 108 (2007)
178. J. Ahrens, et al., Eur. Phys. Lett. A **47**, 36 (2011)
179. M. Oberle, Master Thesis, Univ. Basel (2010) (to be published)
180. F. Pheron, Ph.D. Thesis, Univ Basel (2010) (to be published)
181. N.N. Shevvhenko, et al., Nucl. Phys. A **714**, 277 (2002)
182. A. Fix, H. Arenhövel, Phys. Rev. C **68**, 044002 (2003)
183. L. Tiator, C. Bennhold, S.S. Kamalov Nucl. Phys. A **580**, 455 (1994)
184. K. Nakamura, et al., J. Phys. G **37**, 075021 (2010)
185. Y. Magrhbi, Ph.D. Thesis, Univ. Basel (2010) (to be published)